A Novel ERANOS Procedure for Sensitivity Analyses in Core Depletion Problems: Implementation Details and Verification

A novel ERANOS procedure for sensitivity analyses in core depletion problems: implementation details and verification

Matteo Stanzani,[*,a,b] Donato M. Castelluccio,[b] Francesco Lodi,[b] Vincenzo G. Peluso,[b] Giacomo Grasso,[b] and Marco Sumini[a,c]

[a] *University of Bologna, Department of Industrial Engineering (DIN), Laboratorio di Montecuccolino, Via dei Colli, 16, 40136 Bologna BO, Italy*

[b] *Italian National Agency for New Technologies, Energy and Sustainable Economic Development (ENEA), Centro Ricerche ENEA Bologna, Via dei Mille, 21, 40121 Bologna BO, Italy*

[c] *National Institute for Nuclear Physics (INFN), Viale C. Berti Pichat, 6/2, 40127 Bologna BO, Italy*

[*]Email: matteo.stanzani3@unibo.it

Number of pages: 44
Number of tables: 4
Number of figures: 11

Abstract

Depletion calculations and related sensitivity analyses are fundamental in designing nuclear reactors. Looking at the core design of liquid metal cooled fast reactors, a novel procedure, based on the Generalized Perturbation Theory (GPT), was developed and implemented in the deterministic ERANOS suite to extend its current capabilities related to depletion-related sensitivity analysis. Specifically, a partial perturbative coupling of the burnup equations was introduced to estimate the sensitivities of final isotopic concentrations to microscopic cross sections. First, the procedure was successfully verified through a simple test case by comparing its results with an analytical solution obtained via MATLAB©. Then, a more complex case was studied to highlight the differences between the new perturbatively coupled configuration and the default decoupled one. Overall, the coupling proved to have a non-negligible impact on the sensitivity coefficients, opening the path for further extending the procedure and applying it to more realistic problems.

Keywords — Perturbation Theory, Fuel Depletion, Sensitivity Analysis, Boltzmann-Bateman Coupling, Liquid Metal Cooled Fast Reactors

I. INTRODUCTION

During the core design phase of nuclear reactors, depletion calculations play a fundamental role. They predict the long-term evolution of nuclear reactors, enabling the optimization of fuel loading, the planning of refueling strategies, and providing insight into how changes in the core composition affect performance and efficiency, ultimately ensuring safety. Equally important is sensitivity analysis, which provides information on how perturbations propagate from input design data to output quantities of interest through the calculation of sensitivity coefficients. These coefficients can then be used to explore alternative core configurations or, in combination with input variance and covariance data, to estimate output uncertainties, which are essential for defining safety margins.

The sensitivity analysis can be particularly valuable when applied to depletion calculations, where the propagation of perturbations has a notably intricate impact due to the complex interplay between neutron and nuclide fields over time. The primary challenge lies in the nonlinear coupling of the equations governing the burnup process:

- The Boltzmann equation which describes the shape of the neutron flux.
- The Bateman equation which governs isotopic evolution.
- The power normalization equation, which ensures that the magnitude of the flux is at an appropriate level to produce a desired thermal power.

This non-linearity stems from the presence of products between the neutron flux and the nuclide concentrations in all those equations, which must be solved simultaneously. In general, sensitivity coefficients can primarily be determined through different approaches. The first involves performing and combining calculations for the reference state and the perturbed state associated with the input variation. This direct approach is applicable to both stochastic and deterministic codes. The second approach calculates the coefficients analytically and is particularly suited to deterministic calculations. Concerning the second method, the depletion-related sensitivity coefficients can be obtained by applying the Generalized Perturbation Theory (GPT) to the non-linearly coupled burnup equations, and this is usually done after linearizing with some approximations, so to make them numerically solvable. Different equivalent GPT approaches have been used over the years. In [1], a

variational method based on the minimization of a constrained neutronic property response functional was used, with the burnup equations serving as constraints. Using a differential approach, in [2] sensitivities were obtained and applied to a fast breeder reactor for bi-linearly weighted neutronic properties, which necessitated including the adjoint Boltzmann equation for the neutron importance among the constraints. An improvement on the constant flux depletion approximation adopted in [1] was made in [3], in which the variational GPT formulation assumes a linearly varying flux for the Bateman equation (constant power depletion). The latter was used in [4] to treat the equilibrium burnup cycle. Another method to derive the sensitivity coefficients is through a heuristic approach [5] [6], which relies on the application of conservation principles. The advantages of having formulae for sensitivity coefficients are twofold. First, they are computationally efficient, as they allow for the prediction of the impact of input perturbations on a reference state without performing direct perturbation calculations. Second, they contain important physical insights that enable a deeper analysis of the phenomena involved. These advantages stem from the presence of adjoint quantities, which arise when applying GPT. Depending on the constraints applied, the perturbative coupling of the burnup equations, which manifests in a coupling of adjoints, varies. When only the Bateman equation is used as a constraint, the burnup equations are coupled in the depletion calculation but remain uncoupled for sensitivity computations. This means that while the neutron flux can influence the evolution of nuclides and vice versa, the effects of perturbed fluxes due to altered input data are not accounted for in the sensitivity calculations. Configurations that involve all possible constraints represent the fully perturbatively coupled case. Intermediate configurations lead to partial perturbative couplings. The complexity of the coupled burnup equations is carried over to the sensitivity calculations, and together this limits their current application in nuclear codes. For Monte Carlo codes, there is a general lack of tools for the computation of adjoint-based depletion sensitivity coefficients. A method for computing these coefficients in a full perturbatively coupled configuration was derived and tested for final isotopic concentrations in [7], combining Monte Carlo and depletion simulations. In other works, stochastic calculations obtained using SERPENT2 [8] were blended with deterministic tools through Python for the computation of depletion sensitivities [9] [10]. For deterministic codes, full perturbatively coupled calculations were performed in relation to decay heat using APOLLO3® [11] and MENDEL [12] in [13], where the derivation of the equations used a variational approach similar to that of [1]. For fast reactors,

one of the reference tools is the deterministic European Reactor Analysis Optimized Calculation System (ERANOS) [14], whose latest available release is the 2.3N version (precisely, NEA-1683 ERANOS 2.3N). This version, while able to conduct time-independent sensitivity analyses, has some limitations with respect to depletion. Attempts to increase the functionalities of a previous ERANOS release, version 2.1, were developed and tested with a heuristic approach in [15] for Generation IV reactors. With [16], the perturbatively decoupled case was officially implemented in the source of the 2.3N version for a wide range of response functionals, again adopting the variational approach with constant flux depletion as in [1]. Following the work of [16], an unreleased version of ERANOS was developed with minor modifications to enable full perturbative coupling, as indicated in [17]. Given the current limitations, the aim of this work is to improve the capabilities of the official release of ERANOS 2.3N by introducing a novel procedure (actually, a system of procedures) that accounts for a perturbative coupling of the burnup equations for the computation of sensitivity coefficients. This implementation does not involve modifying the source code, since it consists only of input scripts (written in the ERANOS native Language Utilisateur, or LU) that utilize and combine existing ERANOS functions. The new routine is built on the basis of the GPT variational approach with constant flux depletion, as described in [1] and [13], and allows for a partial perturbative coupling of the burnup equations, which is obtained by considering both the Bateman and the power normalization equations as constraints. This work introduces a novel contribution to the ERANOS environment and employs an innovative way of defining and computing some of the quantities involved. This approach stems from the necessity of not modifying the ERANOS source code and leverages formal similarities in the theoretical equations, which become even more evident when numerical discretizations are applied. In Section II, the theory regarding the direct and the full perturbative couplings of the burnup equations is presented with a general and cohesive approach, the related sensitivity coefficients are derived, and the main features of the novel procedure are described, showing how the formal similarities inherent in the theory were exploited. The correct implementation of the procedure was verified by comparing its results for a simple case with those coming from a MATLAB© analytic calculation. Then, it was applied to a more complex case in ERANOS only to highlight the differences with the perturbatively uncoupled configuration. The tests and their results are presented and discussed in Section III. This work ends with the conclusions and the future perspectives in Section IV.

II. SENSIVITY ANALYSIS FOR DEPLETION PROBLEMS VIA FIRST-ORDER GPT

One of the main challenges in depletion problems arises from the nonlinear coupling of the equations involved, which are collectively called the burnup equations, which makes them impractical to solve without appropriate approximations. The primary equation is the time-dependent Boltzmann equation, which provides the solution in the form of the angular or scalar neutron flux Φ. The second one is the Bateman equation, which describes the time-evolution of the nuclides' vector $\vec{N}$. The third equation is the power normalization equation, used in conjunction with the Boltzmann equation to adjust the flux magnitude to produce a desired thermal power output P. The nonlinear coupling arises from the presence of both the neutron flux and the nuclides' concentrations across all equations, necessitating simultaneous solutions.

II.A. The quasi-static burnup equations

To numerically handle the burnup equations, a widely used approach is to linearize them via the quasi-static approximation. This method involves dividing the depletion period into J discrete time intervals (steps), with each interval spanning from t_j to t_{j+1}. By leveraging the differing time constants of the equations involved, this approximation simplifies the problem, allowing for a more manageable solution. Below, the burnup equations under the quasi-static approximation and their resolution process are described.

II.A.1. Neutron flux

The flux is assumed to vary slowly, allowing it to be approximated by a step-wise constant function. This function is updated only at the beginning of each time step t_j based on the isotopic concentration vector $\vec{N} = [N_1, ..., N_i, ..., N_I]$ at t_j. Consequently, the time-dependent Boltzmann equation simplifies to a pseudo-stationary form. Since it is a homogeneous equation, the neutron flux that solves it is defined in shape, but not in magnitude. Therefore, the pseudo-stationary Boltzmann equation is used to find the flux shape only. Given position $\vec{r}$, neutron energy E, neutron direction $\hat{\Omega}$, and instant t_j, it is given by:

$$\left(\mathcal{A}\big(\vec{N}(\vec{r},t_j),\vec{\sigma}(\vec{r},E,\hat{\Omega})\big) - \frac{1}{k(t_j)}\mathcal{F}\big(\vec{N}(\vec{r},t_j),\vec{\sigma}(\vec{r},E,\hat{\Omega})\big)\right)\psi(\vec{r},E,\hat{\Omega},t_j) = 0, \tag{1}$$

where ψ is the flux shape, $\mathcal{A}$ is the transport, removal, and scattering operator, $\mathcal{F}$ is the fission source operator, $\vec{\sigma}$ is the vector of microscopic cross sections, and $k(t_j)$ is the instantaneous multiplication factor, which is the inverse of the fundamental mode eigenvalue $\lambda(t_j)$. For simplicity, the angular dependence will be omitted hereafter, and the associated $\hat{\Omega}$-integrated quantities will be considered instead. Additionally, the notations $\square_j$ and $\square(t_j)$ will be used interchangeably, depending on convenience. The intensity of the flux shape is set to respect the following normalization condition:

$$\int_0^\infty \int_{\text{reactor}} \psi(\vec{r}, E, t_j)\, d\vec{r}\, dE = 1. \tag{2}$$

Then, the proper flux magnitude $\phi(t_j)$ is obtained upon exploitation of the power normalization equation:

$$P = \phi(t_j) \int_0^\infty \int_{\text{reactor}} \big(\vec{N}(\vec{r}, t_j) \cdot \vec{\sigma}^{(\kappa)}(\vec{r}, E)\big)\psi(\vec{r}, E, t_j)\, d\vec{r}\, dE, \tag{3}$$

in which $\vec{\sigma}^{(\kappa)}$ is the vector that accounts for the kinetic energy released to matter (chiefly coming from fission and capture reactions) by the corresponding isotopes in $\vec{N}$. Isolating ϕ gives:

$$\phi(t_j) = \frac{P}{\int_0^\infty \int_{\text{reactor}} \big(\vec{N}(\vec{r}, t_j) \cdot \vec{\sigma}^{(\kappa)}(\vec{r}, E)\big)\psi(\vec{r}, E, t_j)\, d\vec{r}\, dE}. \tag{4}$$

The scalar neutron flux required to produce P at t_j is then computed as:

$$\Phi(\vec{r}, E, t_j) = \phi(t_j)\psi(\vec{r}, E, t_j). \tag{5}$$

II.A.2. Isotopic evolution

Once the flux has been calculated for step j, it is used as a fixed input in the Bateman equation to evolve the isotopic concentrations from t_j^+ to t_{j+1}^-:

$$\frac{\partial}{\partial t}\vec{N}(\vec{r}, t) = \left(\int_0^\infty \boldsymbol{T}\big(\Phi(\vec{r}, E, t_j), \vec{\sigma}(\vec{r}, E)\big) dE + \boldsymbol{D}(\vec{\Lambda}) \right) \vec{N}(\vec{r}, t), \tag{6}$$

where $\vec{\Lambda}$ is the vector of decay constants, while $\boldsymbol{T}$ and $\boldsymbol{D}$ are the transmutation matrix at $(\vec{r}, E)$ and the decay matrix, respectively. $\boldsymbol{T}$ involves fission yields as well. Notice that the concentrations are continuous at time boundaries, so $\vec{N}(t_j^-) = \vec{N}(t_j) = \vec{N}(t_j^+)$. For simplicity, it is assumed here that there is no external addition or removal of material during the depletion period. This means

that any concentration changes are solely attributable to transmutation and decay phenomena.

II.A.3. Considerations

The described procedure is repeated throughout the entire burnup period for each step, with a final flux update at t_{J+1} often included as well. It is summarized in Figure 1. Two important

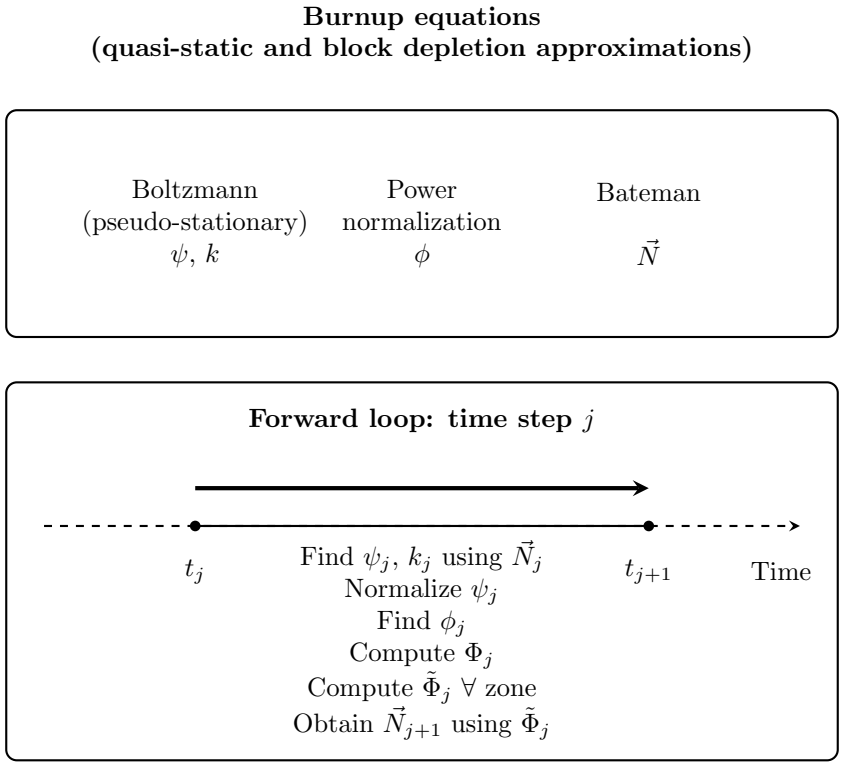

Fig. 1. Schematic representation of the burnup equations and a related step of the forward loop utilized for solving them under the quasi-static and the block depletion approximations. Each equation is accompanied by its associated quantities: ψ and k for the pseudo-stationary Boltzmann equation, ϕ for the power normalization constraint, and $\vec{N}$ for the Bateman equation. For the generic j-th step, the main passages are summarized with the help of the time axis.

points should be highlighted:

- The quasi-static approximation separates the timing of flux and the concentrations' updates, effectively linearizing the burnup equations. In this approach, the Φ calculation treats $\vec{N}$ as a fixed input while $\vec{N}$ is updated based on a fixed flux. This linearization simplifies the calculation process by decoupling the temporal updates of flux and concentrations.

- The adoption of a constant flux depletion implies that the exact power production P is

ensured only at the boundaries of time steps. Although the calculation uses linearized equations, it still represents a nonlinear process [1].

Additionally, the numerical resolution of the quasi-static burnup equations requires discretization in space (spatial grid composed of mesh elements e), energy (multi-group representation), and neutron direction. Numerically solving the Boltzmann equation makes the neutron flux available at each mesh element. However, since the Bateman equation is challenging to solve with a refined grid, it is typically treated using block depletion [1]. The reactor is divided into Z zones, and zone-averaged fluxes $\tilde{\Phi}$ are prepared for use in the discretized version of Eq. 6, with the averaging being performed using the volumes of the mesh elements belonging to each zone. Note also that all input nuclear data are provided for each zone, not for each mesh element. The block depletion simplifies the problem, thereby making the computation of isotopic concentrations more manageable. The difference between the grid and zone levels is displayed, for a simple case with sixteen mesh elements and two reactor zones, in Figure 2.

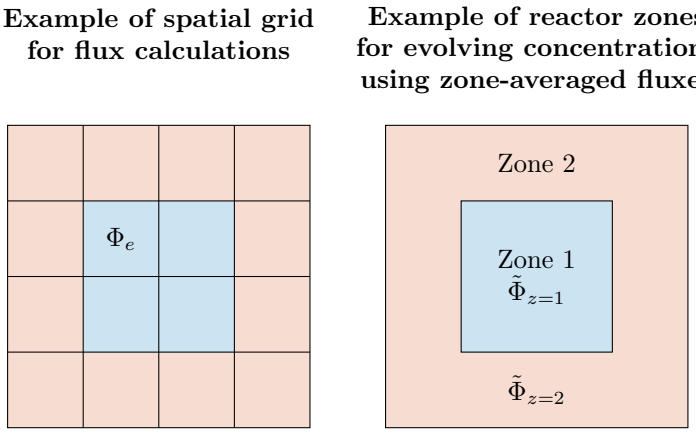

Fig. 2. A simple example illustrating the different levels at which the Boltzmann and the Bateman equations are typically solved in deterministic codes. On the left, the neutron flux is available at each mesh element e of the fine spatial grid, with the generic notation Φ_e. However, to utilize this flux for updating isotopic concentrations, it must first undergo a zone-averaging process. This averaging is performed separately for each macro reactor zone, as shown on the right. Consequently, at any given moment, isotopic concentrations are uniform across all mesh elements within the same zone.

II.B. The adjoint equations for sensitivity analysis

After applying the quasi-static approximation to perform the depletion calculation, an additional procedure can be followed to obtain first-order sensitivity coefficients S in the context of a sensitivity analysis. To derive the sensitivities, a variational approach is adopted in this work. It revolves around minimizing a constrained functional and involves adjoint quantities as Lagrange multipliers. The variational approach of GPT for depletion problems is summarized below based on [1] and [13], followed by an overview of the associated novel ERANOS functionalities.

II.B.1. Construction of a constrained response functional using the burnup equations

For a generic response functional F and any input parameter α, $S(F,\alpha)$ is defined as

$$S(F,\alpha) = \frac{\delta F}{F} \Big/ \frac{\delta \alpha}{\alpha} = \frac{\alpha}{F}\frac{\partial F}{\partial \alpha}, \tag{7}$$

providing information about the relative variation of F caused by the propagation of a small perturbation $\delta\alpha$. The functional used for the sensitivity coefficients in this work is labeled as K and it can be derived starting from the following generic functional R:

$$R(\vec{\phi},\vec{\psi},\vec{N},\vec{\alpha}) = \int_{t_1}^{t_{J+1}} \int_0^{\infty} \int_{\text{reactor}} \mathcal{R}(\vec{\phi},\vec{\psi},\vec{N},\vec{\alpha})\, d\vec{r}\, dE\, dt, \tag{8}$$

where $\mathcal{R}$ is the integrand related to the functional, $\vec{\phi} = [\phi(t_1), ..., \phi(t_{J+1})]$, $\vec{\psi} = [\psi(t_1), ..., \psi(t_{J+1})]$, and $\vec{\alpha} = [\alpha_1, ..., \alpha_m, ..., \alpha_M]$ is the vector of input parameters. Of particular interest are the responses at the end of the depletion period (final responses), which are obtained by using $\delta(t-t_f)$ as a weighting function for $\mathcal{R}$ in the time integral, with $t_f = t_{J+1}$ being used to indicate the final instant of depletion. Even though the theoretical part will remain general to include all possible R, only final isotopic concentrations will be considered as responses for the numerical calculations presented in this work. For instance, for the generic isotope i at position $\vec{r}_p$, the corresponding final response can be written as:

$$R(N_i) = \int_{t_1}^{t_f} \int_{\text{reactor}} N_i(\vec{r},t)\delta(\vec{r}-\vec{r}_p)\delta(t-t_f)\, d\vec{r}\, dt = N_i(\vec{r}_p,t_f). \tag{9}$$

Returning to the general case, the functional K corresponds to the constrained version of Eq. (8), where the quasi-static burnup equations (including the flux shape normalization condition) are used as constraints, and appended to R with fixed Lagrange multipliers:

$$K(\vec{\phi},\vec{\psi},\vec{N},\vec{\lambda},\vec{\alpha}) = R + \sum_{j=1}^{J}\int_{t_{j^+}}^{t_{j+1}^-}\left\langle \vec{N}^*, \left(-\frac{\partial}{\partial t} + [\boldsymbol{T}_j]_E + \boldsymbol{D}\right)\vec{N}\right\rangle_{\vec{r}} dt$$

$$-\sum_{j=1}^{J+1}\left\langle \Gamma_j^*, \left(\mathcal{A}_j - \lambda_j \mathcal{F}_j\right)\psi_j\right\rangle_{\vec{r},E} - \sum_{j=1}^{J+1} P_j^*\left(\phi_j\left[\vec{N}_j\cdot\vec{\sigma}^{(\kappa)}\psi_j\right]_{\vec{r},E} - P\right) - \sum_{j=1}^{J+1} a_j^*\left(\left[\psi_j\right]_{\vec{r},E} - 1\right), \quad (10)$$

where $\vec{\lambda}$ is the vector of instantaneous eigenvalues, and the vectorized Lagrange multipliers are $\vec{N}^*$, $\vec{\Gamma}^*$, $\vec{P}^*$, and $\vec{a}^*$. Notation-wise, $\langle\cdot,\cdot\rangle_\square$ and $[\,\cdot\,]_\square$ are both integrals with respect to $\square$, but the former indicates an inner product specifically, according to the Dirac notation. Note that the constraints are all identically 0, as they are built with equations, leading to K and R having identical numerical values. The form of Eq. (10) is almost identical to the one used in [1], except for the fact that the last three constraints consider also the time instant t_{J+1}, similarly to what is done in [13]. The Lagrange multipliers are defined by the associated Euler equations [1], which are linked to the condition of K being stationary with respect to variations of the functions and the eigenvalues it involves. To find them, the initial step involves computing the first-order differential dK. This can be achieved either by direct differentiation or, equivalently, by performing a Taylor expansion around the unperturbed state K to account for a perturbed state K' resulting from a small variation $\delta\vec{\alpha}$. Either approach leads to:

$$dK = \sum_{j=1}^{J+1}\frac{\partial K}{\partial \phi_j}d\phi_j + \sum_{j=1}^{J+1}\left[\frac{\partial K}{\partial \psi_j}d\psi_j\right]_{\vec{r},E} + \sum_{j=1}^{J}\int_{t_j^+}^{t_{j+1}^-}\left[\frac{\partial K}{\partial \vec{N}}\cdot d\vec{N}\right]_{\vec{r}} dt$$

$$+\sum_{j=1}^{J+1}\frac{\partial K}{\partial \lambda_j}d\lambda_j + \sum_{m=1}^{M}\frac{\partial K}{\partial \alpha_m}d\alpha_m. \quad (11)$$

The sensitivity coefficient $S(K,\alpha)$ is thus related to the computation of $\partial K/\partial\alpha$, with $\alpha = \alpha_m$ for simplicity of notation.

II.B.2. The adjoint power equation

The Lagrange multiplier $P_j^* = P^*(t_j)$, known as the adjoint power at t_j, is defined by enforcing the $d\phi_j$ term in Eq. (11) to vanish. This is achieved by computing the derivative of Eq. (10) with respect to ϕ_j and setting it to 0. Exploiting Eq. (3) and the linearity of the transmutation matrix with respect to the flux magnitude, the Euler equation for the adjoint power at t_j is given by:

$$P_j^* = \frac{\phi_j}{P}\frac{\partial R}{\partial \phi_j} + \frac{1}{P}\int_{t_{j^+}}^{t_{j+1}^-} \left\langle \vec{N}^*, [\boldsymbol{T}_j]_E \vec{N} \right\rangle_{\vec{r}} dt, \tag{12}$$

in which the second term on the right-hand side is not to be considered if $j = J + 1$, since it would fall outside the depletion period. Physically, the adjoint power P_j^* is the importance of a perturbation of the flux intensity, $\delta\phi(t_j)$, to the response functional [1].

II.B.3. The generalized adjoint flux equation

The Euler equation for the Lagrange multiplier $\Gamma_j^* = \Gamma^*(\vec{r}, E, t_j)$, namely the generalized adjoint flux at t_j, is related to the canceling of $\partial K/\partial \psi_j$. Applying the commutation property of adjoint operators to the Boltzmann constraint of Eq. (10) gives:

$$\left\langle \Gamma_j^*, \left(\mathcal{A}_j - \frac{\mathcal{F}_j}{k_j}\right)\psi_j \right\rangle_{\vec{r},E} = \mathcal{J}(\Gamma_j^*, \psi_j^*) + \left\langle \left(\mathcal{A}_j^* - \frac{\mathcal{F}_j^*}{k_j}\right)\Gamma_j^*, \psi_j \right\rangle_{\vec{r},E}, \tag{13}$$

in which $\mathcal{J}(\Gamma_j^*, \psi_j)$ is the bilinear concomitant, while $\mathcal{A}_j^*$ and $\mathcal{F}_j^*$ are the operators adjoint to $\mathcal{A}_j$ and $\mathcal{F}_j$, respectively. Imposing that $\mathcal{J} = 0$ leads to the boundary conditions for Γ_j^*. They coincide with those usually adopted for the neutron importance function Φ^* [1]. Substituting Eq. (13) into Eq. (10) and forcing its derivative with respect to ψ_j to be 0 results in the Euler equation for the generalized adjoint flux:

$$\left(\mathcal{A}_j^* - \frac{\mathcal{F}_j^*}{k_j}\right)\Gamma_j^* = Q_j^*, \tag{14}$$

where

$$Q_j^* = \frac{\partial R}{\partial \psi_j} + \int_{t_{j^+}}^{t_{j+1}^-} \left(\vec{N}^*, \frac{\partial \boldsymbol{T}_j}{\partial \psi_j}\vec{N}\right) dt - P_j^* \phi_j \vec{N}_j \cdot \vec{\sigma}^{(\kappa)} - a_j^* \tag{15}$$

is the generalized adjoint source. Similarly to Eq. (12), the second term on the right-hand side of Eq. (15) is 0 if $j = J + 1$. The generalized adjoint source obeys the orthogonality condition

$$\left\langle Q_j^*, \psi_j \right\rangle_{\vec{r},E} = 0, \tag{16}$$

which comes from the Boltzmann constraint making use of Eqs. (1), (13), and (14). Forcing $\partial K/\partial \lambda_j = 0$ leads to another orthogonality condition, between the generalized adjoint flux and the fission term of the Boltzmann equation:

$$\left\langle \Gamma_j^*, \mathcal{F}_j \psi_j \right\rangle_{\vec{r},E} = 0. \tag{17}$$

This is possible only if Γ_j^* contains no fundamental mode i.e., if it does not involve the neutron importance function, which is the solution to the homogeneous version of Eq. (14). In general, if $\Gamma_{j,P}^*$ is a particular solution of Eq. (14), then $\Gamma_j^* = \Gamma_{j,P}^* + \xi \Phi_j^*$, with ξ an arbitrary scalar, is also a solution. However, since $\mathcal{F}_j \psi_j$ could be 0 or not 0 depending on position and energy, ξ has to be 0 to respect the orthogonality condition of Eq. (17) [1], i.e. the fundamental mode Φ_j^* must be filtered out. In ERANOS, for instance, this can be ensured by properly setting the flux solver [18]. From a physical point of view, Γ_j^* represents the importance of a perturbation on the flux shape, $\delta\psi(t_j)$, to the response functional [1].

II.B.4. The adjoint Bateman equation

The Lagrange multiplier associated with the isotopic evolution is the vector of adjoint concentrations $\vec{N}^* = \vec{N}^*(\vec{r}, t)$. The Euler equation in this case is found from $\partial \vec{K}/\partial \vec{N}$. Before computing the derivative, the Bateman constraint in Eq. (10) is rewritten using the commutation property of adjoint operators, which in this case involves one integration by parts and the transposed of the transmutation and the decay matrices:

$$\sum_{j=1}^{J} \int_{t_{j+}}^{t_{j+1}^-} \left\langle \vec{N}^*, \left(-\frac{\partial}{\partial t} + [\boldsymbol{T}_j]_E + \boldsymbol{D} \right) \vec{N} \right\rangle_{\vec{r}} dt$$

$$= \sum_{j=1}^{J} \left(-\left[\vec{N}^* \cdot \vec{N} \right]_{\vec{r}} \Big|_{t_j^+}^{t_{j+1}^-} + \int_{t_{j+}}^{t_{j+1}^-} \left\langle \left(+\frac{\partial}{\partial t} + [\boldsymbol{T}_j^*]_E + \boldsymbol{D}^* \right) \vec{N}^*, \vec{N} \right\rangle_{\vec{r}} dt \right), \tag{18}$$

where the first term on the right-hand side is the bilinear concomitant for step j, while $\boldsymbol{T}^*$ and $\boldsymbol{D}^*$ are the transposed matrices of $\boldsymbol{T}$ and $\boldsymbol{D}$, respectively. The Euler equation for $\vec{N}^*$ related to step j is found by computing the derivative of Eq. (10) with respect to $\vec{N}$ and imposing the vanishing of the terms that involve time integrals. The following is obtained:

$$-\frac{\partial \vec{N}^*}{\partial t} = \left([\boldsymbol{T}_j^*]_E + \boldsymbol{D}^*\right)\vec{N}^* + \frac{\partial R}{\partial \vec{N}}, \tag{19}$$

which is called the adjoint Bateman equation and is to be solved backward in time for t between t_{j+1} and t_j, as suggested by the negative time derivative. The remaining terms in $\partial K/\partial \vec{N}$ refer to time boundaries only. They are required to vanish as well to ensure that K is stationary with respect to $\vec{N}$. If a discontinuity is allowed in the adjoint concentration vector at t_j for $j = 2, ..., J$, i.e. $\vec{N}^*(t_j^-) \neq \vec{N}^*(t_j^+)$, the sum of the bilinear concomitants appeared in Eq. (18) can be written as

$$-\sum_{j=1}^{J} \left(\vec{N}^* \cdot \vec{N}\right)\Big|_{t_j^+}^{t_{j+1}^-} = \vec{N}^*(t_1^+) \cdot \vec{N}(t_1)$$

$$-\Big(\left(\vec{N}^*(t_2^-) - \vec{N}^*(t_2^+)\right) \cdot \vec{N}(t_2) + ... + \left(\vec{N}^*(t_{J-1}^-) - \vec{N}^*(t_J^+)\right) \cdot \vec{N}(t_J)\Big) - \vec{N}^*(t_{J+1}^-) \cdot \vec{N}(t_{J+1}), \tag{20}$$

where the continuity of $\vec{N}$ has been exploited and the presence of a space integration has been removed by the derivative. From the discontinuity assumption, a jump condition is obtained at $t_{j+1} = t_2, ..., t_{J-1}$, which is to be used as a final condition in the correspondent step j for solving Eq. (19):

$$\vec{N}^*(\vec{r}, t_{j+1}^-) = \vec{N}^*(\vec{r}, t_{j+1}^+) - \left\langle \Gamma_{j+1}^*, \left(\frac{\partial \mathcal{A}_{j+1}}{\partial \vec{N}(t_{j+1})} - \frac{1}{k_{j+1}} \frac{\partial \mathcal{F}_{j+1}}{\partial \vec{N}(t_{j+1})}\right)\psi_{j+1} \right\rangle_E - P_{j+1}^* \phi_{j+1} \left[\vec{\sigma}^{(\kappa)} \psi_{j+1}\right]_E, \tag{21}$$

where $-P_{j+1}^* \phi_{j+1} \left[\vec{\sigma}^{(\kappa)} \psi_{j+1}\right]_E$ is the power jump term that connects the adjoint power and the adjoint concentration vector at t_{j+1}. The vector $\phi_{j+1} \left[\vec{\sigma}^{(\kappa)} \psi_{j+1}\right]_E$ will be also indicated as $\vec{\Pi}_{j+1}$. In analogy, the second term on the right-hand side of Eq. (21) is the flux shape jump term. For $t_{j+1} = J + 1$, a final condition similar to Eq. (21) is found:

$$\vec{N}^*(\vec{r}, t_{J+1}^-) = -\left\langle \Gamma_{J+1}^*, \left(\frac{\partial \mathcal{A}_J}{\partial \vec{N}} - \frac{1}{k_J} \frac{\partial \mathcal{F}_{J+1}}{\partial \vec{N}}\right)\psi_{J+1} \right\rangle_E - P_{J+1}^* \phi_{J+1} \left[\vec{\sigma}^{(\kappa)} \psi_{J+1}\right]_E. \tag{22}$$

For $j = 1$, since each element of $\vec{N}(\vec{r}, t_1)$ is an input quantity that can be considered as a possible α, the corresponding term is not forced to be 0, but it is instead retained as part of the sensitivity coefficient. If α is the initial concentration $N_i(\vec{r}, t_1)$ of isotope i, then

$$S(K, N_i(\vec{r}, t_1)) = \frac{N_i(\vec{r}, t_1)}{R}\Bigg(- \left\langle \Gamma_1^*, \left(\frac{\partial \mathcal{A}_1}{\partial N_i(\vec{r}, t_1)} - \frac{1}{k_1} \frac{\partial \mathcal{F}_1}{\partial N_i(\vec{r}, t_1)} \right) \psi_1 \right\rangle_E$$

$$- P_1^* \phi_1 \left[\sigma_i^{(\kappa)} \psi_1 \right]_E + N_i^*(\vec{r}, t_1^+) \Bigg), \tag{23}$$

where R has been used in place of K as they have the same numerical value. From a physical point of view, similarly to the other adjoints, $\vec{N}^*(\vec{r}, t)$ represents the importance that a change $\delta\vec{N}(\vec{r}, t)$ has for the response functional [1].

II.C. The sensitivity coefficient

The sensitivity coefficient $S(K, \alpha)$, for α different from initial concentrations, is obtained from the computation of $\partial K/\partial\alpha$:

$$S(K, \alpha) = \frac{\alpha}{K}\frac{\partial K}{\partial \alpha} = \frac{\alpha}{R}\frac{\partial K}{\partial \alpha} = \frac{\alpha}{R}\Bigg\{ \frac{\partial R}{\partial \alpha} + \sum_{j=1}^{J} \int_{t_{j+}}^{t_{j+1}^-} \left\langle \vec{N}^*, \left(\frac{\partial [\boldsymbol{T}_j]_E}{\partial \alpha} + \frac{\partial \boldsymbol{D}}{\partial \alpha} \right) \vec{N} \right\rangle_{\vec{r}} dt$$

$$- \sum_{j=1}^{J+1} \left\langle \Gamma_j^*, \left(\frac{\partial \mathcal{A}_j}{\partial \alpha} - \frac{1}{k_j} \frac{\partial \mathcal{F}_j}{\partial \alpha} \right) \psi_j \right\rangle_{\vec{r},E} - \sum_{j=1}^{J+1} P_j^* \left(\phi_j \left\langle \vec{N}_j \cdot \frac{\partial \vec{\sigma}^{(\kappa)}}{\partial \alpha} \psi_j \right\rangle_{\vec{r},E} \right) \Bigg\}, \tag{24}$$

where, based on the dependencies of α, space and/or energy integrals could vanish. For instance, if $\alpha = \alpha(\vec{r}, E)$, as is the case with microscopic cross sections, then Eq. (24) becomes

$$S(K, \alpha) = \frac{\alpha}{R}\Bigg\{ \frac{\partial R}{\partial \alpha} + \sum_{j=1}^{J} \int_{t_{j+}}^{t_{j+1}^-} \left(\vec{N}^*, \frac{\partial \boldsymbol{T}_j}{\partial \alpha} \vec{N} \right) dt$$

$$- \sum_{j=1}^{J+1} \left(\Gamma_j^*, \left(\frac{\partial \mathcal{A}_j}{\partial \alpha} - \frac{1}{k_j} \frac{\partial \mathcal{F}_j}{\partial \alpha} \right) \psi_j \right) - \sum_{j=1}^{J+1} P_j^* \phi_j \vec{N}_j \cdot \frac{\partial \vec{\sigma}^{(\kappa)}}{\partial \alpha} \psi_j \Bigg\}. \tag{25}$$

In both formulae, $S_D(R, \alpha) = \partial R/\partial\alpha$ is the direct term, while the others are the indirect ones. In order, they are the Bateman, the flux shape, and the power (or flux magnitude) terms. They are respectively labeled with $S_N(R, \alpha)$, $S_\psi(R, \alpha)$, and $S_P(R, \alpha)$, so that each subscript recalls a constraint to be satisfied, allowing for the use of R in place of K in the brackets. Below, $S(K, \alpha)$ and

$S(R, \alpha)$ will be used interchangeably since the status of the constraints will be assumed implicitly.

II.C.1. Perturbative coupling and adjoint procedure description

The functional K was constructed considering all the quasi-static burnup equations as constraints. This results in a full perturbative coupling, where the adjoint quantities $\vec{N}^*$, $\vec{P}^*$, $\vec{\Gamma}^*$ and $\vec{a}^*$ are interdependent. If the two constraints related to the flux shape are removed, the perturbative coupling becomes partial, involving only concentrations and flux magnitude through $\vec{N}^*$ and $\vec{P}^*$. If, additionally, the power normalization equation is not considered in Eq. (10), then the depletion problem is perturbatively decoupled, as $\vec{N}^*$ does not depend on any other adjoint quantity. A schematic summary of the different perturbative couplings is shown in the upper portion of Figure 3. The perturbatively decoupled depletion problem is currently manageable by some ERANOS 2.3N modules introduced with [16]. However, the novel LU procedures implemented presented in this work aim to achieve the partial and, eventually, the full perturbative coupling. The first part of the procedure consists of a forward loop in time that solves the discretized quasi-static burnup equations (with the computation of zone-averaged fluxes to be used in the Bateman equation, see Figure 2). The adjoint portion of the procedure takes input data from the direct one, is based on a backward loop in time, and involves the computation of sensitivity coefficients. The procedure allows for selectively applying constraints by setting the corresponding Lagrange multipliers to zero. At present, the new algorithm considers only final isotopic concentrations as R. For these specific responses (and for any final response in general), $\partial R/\partial \vec{N}$ can be moved from Eq. (19) to Eq. (22) [1]. Additionally, the following quantities vanish: $\partial R/\partial \psi_j$, $\partial R/\partial \phi_j$, a_j^*, P_{J+1}^*, and Γ_{J+1}^*. For this work, the procedure was verified only for the partial perturbative coupling configuration. However, the calculation of Q_j^*, which pertains to the full coupling, was tested as well in a way that did not affect the other results. In summary, the backward loop used to produce the results presented in this work starts with $j = J$ (indicating step j between t_j and t_{j+1}) and, for a fixed set (R, α), follows these steps (see also the lower portion of Figure 3):

1. Solve Eq. (19) from t_{j+1}^- to t_j^+ to evolve $\vec{N}^*$ using either Eq. (22), if $j+1 = J+1$, or Eq. (21), if $j + 1 < J + 1$, as the final condition.

2. Calculate the S_N component belonging to the j-th time step. Then, update the total S_N with it.

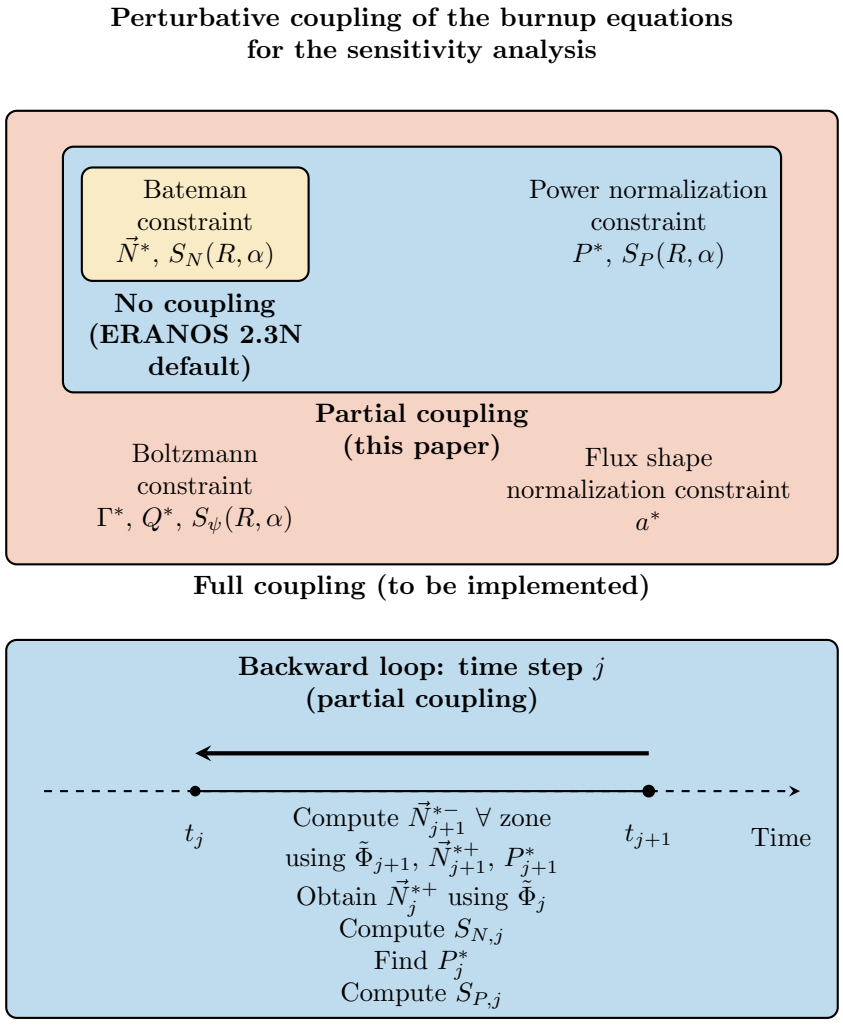

Fig. 3. Schematic representation of the possible perturbative couplings of the burnup equation for computing sensitivity coefficients: no coupling (consider only the Bateman constraint), partial (add the power normalization constraint), or full (consider the Boltzmann and the flux shape normalization constraints). Each constraint is associated with the corresponding adjoint quantity and the indirect sensitivity terms: $\vec{N}^*$ and S_N for the Bateman constraint, P^* and S_P for the power normalization constraint, Γ^* (with the source Q^*) and S_ψ for the Boltzmann constraint, and a^* for the flux shape normalization constraint. When considering the partial perturbative coupling, which is subject of this work, the generic j-th step of the backward loop method is illustrated with reference to the time axis.

3. Solve Eq. (12) to find P^*_j.

4. Calculate Q^*_j with Eq. (15) (for checking purposes only).

5. If $j > 1$, update $\vec{N}^*$ at t^-_j with Eq. (21).

6. Calculate the S_P component belonging to the j-th time step. Then, update the total S_P with it.

7. If $j = 1$, exit the loop, otherwise decrease j by 1.

Notice that, since the Boltzmann constraint is not considered, the jump condition for $\vec{N}^*$ is missing the Γ_j^* term (see Eq. 21), and therefore this ultimately alters the value assumed by Q^*. The peculiar feature of this procedure lies in how P_j^* and Q_j^* are calculated, as they are based on the ERANOS functions dedicated to the computation of $S_{N,j}$, which were introduced in ERANOS 2.3N with [16].

II.D. Implementation of the adjoint power in ERANOS

To implement the adjoint power in ERANOS without modifying the source code, formal similarities have been exploited. In the generic case that α is $\sigma_i^{(x)}(\vec{r}, E)$, i.e. the microscopic cross section of reaction x for isotope i at $(\vec{r}, E)$, the expression for $S_{N,j}$ is given by:

$$S_{N,j}(R, \sigma_i^{(x)}(\vec{r}, E)) = \frac{1}{R} \int_{t_{j+}}^{t_{j+1}^-} \left(\vec{N}^*(\vec{r}, t), \sigma_i^{(x)}(\vec{r}, E) \frac{\partial \boldsymbol{T}_j(\vec{r}, E)}{\partial \sigma_i^{(x)}(\vec{r}, E)} \vec{N}(\vec{r}, t) \right) dt, \tag{26}$$

which is non-zero if the chosen cross section features in the transmutation matrix. As already mentioned, the discretization adopted in ERANOS is so that $\vec{N}$, $\vec{N}^*$, and microscopic cross sections are functions of the reactor zone z. In the transmutation matrix, this requires the use of zone-averaged fluxes. Moreover, the group discretization of energy must be considered. Therefore, Eq. (26) can be rewritten in approximated form as

$$S_{N,j}(R, \sigma_{i,z,g}^{(x)}) = \frac{1}{R} \int_{t_{j+}}^{t_{j+1}^-} \left(\vec{N}_z^*(t), \sigma_{i,z,g}^{(x)} \frac{\partial \tilde{\boldsymbol{T}}_{j,z,g}}{\partial \sigma_{i,z,g}^{(x)}} \vec{N}_z(t) \right) dt, \tag{27}$$

where $\tilde{\boldsymbol{T}}_{j,z,g}$ is the portion of the discretized transmutation matrix that refers to zone z, energy group g and time step j. Since the zone-averaged flux $\tilde{\Phi}_{j,z,g}$ is involved, the $\tilde{\square}$ notation has been introduced for the transmutation matrix as well. Note that, in ERANOS, the time integral is approximated using the mean values of $\vec{N}$ and $\vec{N}^*$ calculated with their values at t_j^+ and t_{j+1}^- [16]. When short-lived nuclides like ^{239}Np are involved in the evolution chain, an appropriate computation of such time integrals can be probably achieved through a combination of highly refined,

non-uniform time steps and the introduction of sub-steps. The latter approach, in particular, would allow for collecting multiple values of N and N^* for each major step without needing to frequently update the flux in the associated sub-steps, which can be time-consuming. Although no short-lived nuclides were included in the cases studied for this work, their impact must be addressed in future studies. In the following, for better clarity, the time integral notation will be kept in place of the actual ERANOS formulation. Now, discretizing Eq. (12) in a similar way to $S_{N,j}$ leads to:

$$P_j^* = \frac{1}{P} \sum_z V_z \int_{t_j^+}^{t_{j+1}^-} \left(\vec{N}_z^*(t), \sum_g \tilde{\boldsymbol{T}}_{j,z,g} \vec{N}_z(t) \right) dt, \tag{28}$$

where V_z is the volume of the reactor zone z. The important thing to highlight at this point is that, since the transmutation matrix is linear in the cross sections, it is possible to write

$$\sum_{i,r} \sigma_{i,z,g}^{(x)} \frac{\partial \tilde{\boldsymbol{T}}_{j,z,g}}{\partial \sigma_{i,z,g}^{(x)}} = \tilde{\boldsymbol{T}}_{j,z,g}. \tag{29}$$

Eq. (28) can then be rewritten exploiting Eq. (29):

$$P_j^* = \frac{1}{P} \sum_z V_z \int_{t_j^+}^{t_{j+1}^-} \left(\vec{N}_z^*(t), \sum_{g,x,i} \sigma_{z,g,i}^{(x)} \frac{\partial \tilde{\boldsymbol{T}}_{z,g,i}}{\partial \sigma_{z,g,i}^{(x)}} \vec{N}_z(t) \right) dt, \tag{30}$$

where the sums are so that all the cross sections appearing in the transmutation matrix are accounted for. From Eqs. (27) and (30) it can be seen that the adjoint power can be rewritten in terms of Bateman sensitivities as

$$P_j^* = \frac{R}{P} \sum_{i,z,g,x} V_z S_{N,j}(R, \sigma_{i,z,g}^{(x)}). \tag{31}$$

This formulation of the adjoint power served as the base for how it was implemented in ERANOS through LU procedures. It can be easily extended to account for flux-dependent responses.

II.E. Implementation of the generalized adjoint source in ERANOS

For responses that are final isotopic concentrations, Q_j^* is the difference between two terms:

$$Q_j^*(\vec{r}, E) = Q_{j,\mathrm{I}}^*(\vec{r}, E) - Q_{j,\mathrm{II}}^*(\vec{r}, E), \tag{32}$$

where

$$Q^*_{j,\mathrm{I}}(\vec{r},E) = \int_{t_{j+}}^{t_{j+1}^-} \left(\vec{N}^*(\vec{r},t), \frac{\partial \boldsymbol{T}_j(\vec{r},E)}{\partial \psi_j(\vec{r},E)} \vec{N}(\vec{r},t) \right) dt, \tag{33}$$

and

$$Q^*_{j,\mathrm{II}}(\vec{r},E) = P^*_j \phi_j(\vec{r},E) \vec{N}_j(\vec{r}) \cdot \vec{\sigma}^{(\kappa)}(\vec{r},E). \tag{34}$$

$Q^*_{j,\mathrm{II}}$ was easy to implement, since P^*_j is available through Eq. (31). For $Q^*_{j,\mathrm{I}}$, the idea was again to use Bateman sensitivities. Discretizing Eq. (33) gives:

$$Q^*_{j,z,g,\mathrm{I}} = \int_{t_{j+}}^{t_{j+1}^-} \left(\vec{N}^*_z(t), \frac{\partial \tilde{\boldsymbol{T}}_{j,z,g}}{\partial \psi_{j,z,g}} \vec{N}_z(t) \right) dt. \tag{35}$$

The transmutation matrix is linear also in the flux shape, and therefore

$$\psi_{j,z,g} \frac{\partial \tilde{\boldsymbol{T}}_{j,z,g}}{\partial \psi_{j,z,g}} = \tilde{\boldsymbol{T}}_{j,z,g}. \tag{36}$$

Exploiting Eq. (36) in Eq. (35) leads to:

$$Q^*_{j,z,g,\mathrm{I}} = \int_{t_{j+}}^{t_{j+1}^-} \left(\vec{N}^*_z(t), \frac{\tilde{\boldsymbol{T}}_{j,z,g}}{\psi_{j,z,g}} \vec{N}_z(t) \right) dt. \tag{37}$$

Then, using Eq. (29), the result is:

$$Q^*_{j,z,g,\mathrm{I}} = \frac{1}{\psi_{j,z,g}} \int_{t_{j+}}^{t_{j+1}^-} \left(\vec{N}^*_z(t), \sum_{i,x} \sigma^{(x)}_{i,z,g} \frac{\partial \tilde{\boldsymbol{T}}_{j,z,g}}{\partial \sigma^{(x)}_{i,z,g}} \vec{N}_z(t) \right) dt, \tag{38}$$

which, in terms of Bateman sensitivities, becomes

$$Q^*_{j,z,g,\mathrm{I}} = \frac{R}{\psi_{j,z,g}} \sum_{i,x} S_{N,j}(R, \sigma^{(x)}_{i,z,g}). \tag{39}$$

Comparing Eq. (31) with Eq. (39) shows that both are based on summations involving Bateman sensitivity terms. In particular, since P^*_j is a single scalar quantity, the summation regards isotopes, energy groups, zones, and reactions. Vice versa, given that $Q^*_{j,\mathrm{I}}$ must be provided in ERANOS for each zone and group, the summation refers only to isotopes and reactions. Moreover, both formulae have multiplication factors for $S_{N,j}$: RV_z/P for Eq. (31), and $R/\psi_{j,z,g}$ for Eq. (39). These structural affinities lead to the implementation in ERANOS of P^* and $Q^*_{j,I}$ through partially

combined subroutines, and this was also the reason for testing the calculation of Q_j^*.

II.F. Implementation of the power sensitivity term in ERANOS

In ERANOS, the kinetic energy released to matter for the generic isotope i at $(\vec{r}, E)$ is given by [19]:

$$\sigma_i^{(\kappa)}(\vec{r}, E) = Q_i^{(c)}\sigma_i^{(c)}(\vec{r}, E) + Q_i^{(f)}\sigma_i^{(f)}(\vec{r}, E)$$

$$-\bar{E}(\vec{r})\big(\nu_i(\vec{r}, E)\sigma_i^{(f)}(\vec{r}, E) - \sigma_i^{(f)}(\vec{r}, E) - \sigma_i^{(c)}(\vec{r}, E)\big), \tag{40}$$

where $Q^{(c)}$ and $Q^{(f)}$ are, respectively, the Q values for capture and fission reactions, ν is the average number of neutrons released by a single fission event, and $\bar{E}$ is the spectrum-weighted neutron incident energy. In discretized form, Eq. (40) becomes:

$$\sigma_{i,z,g}^{(\kappa)} = Q_i^{(c)}\sigma_{i,z,g}^{(c)} + Q_i^{(f)}\sigma_{i,z,g}^{(f)} - \bar{E}_z\big(\nu_{i,z,g}\sigma_{i,z,g}^{(f)} - \sigma_{i,z,g}^{(f)} - \sigma_{i,z,g}^{(c)}\big) \tag{41}$$

The discretized version of the power sensitivity term at t_j that features $\sigma_{i,z,g}^{(\kappa)}$ is:

$$S_{P,j}(R, \sigma_{i,z,g}^{(x)}) = \frac{1}{R}P_j^*\phi_j N_{j,i,z}\left(\sigma_{i,z,g}^{(x)}\frac{\partial\sigma_{i,z,g}^{(\kappa)}}{\partial\sigma_{i,z,g}^{(x)}}\right)\psi_{j,z,g}, \tag{42}$$

which can be nonzero only if (x) is either a capture (c) or a fission (f) reaction. The nature of (x) influences how the bracketed term on the right-hand side is computed. If $(x) = (c)$, then

$$\sigma_{i,z,g}^{(c)}\frac{\partial\sigma_{i,z,g}^{(\kappa)}}{\partial\sigma_{i,z,g}^{(c)}} = \big(Q_i^{(c)} + \bar{E}_z\big)\sigma_{i,z,g}^{(c)}. \tag{43}$$

On the other hand, if $(x) = (f)$, then

$$\sigma_{i,z,g}^{(f)}\frac{\partial\sigma_{i,z,g}^{(\kappa)}}{\partial\sigma_{i,z,g}^{(f)}} = \big(Q_i^{(f)} - \bar{E}_z\big(\nu_{i,z,g} - 1\big)\big)\sigma_{i,z,g}^{(f)}. \tag{44}$$

Given that the $\bar{E}_z$ value is calculated by ERANOS for the preparation of $\vec{\sigma}^{(\kappa)}$, but is not directly accessible, to make it available it has been extracted for each zone using Eq. (41) in reverse mode with a novel dedicated LU subroutine.

III. ANALYTICAL VERIFICATION

The novel ERANOS procedure was applied to 2 test cases of increasing complexity. The first one (Case A) was kept simple enough so an analytic solution could be used to verify the correct coding in ERANOS and quantify the impact of approximations on the numerical solution. The second one (Case B) was more complex, yet still capable of highlighting basic phenomena, and it was used to showcase the physical significance of the perturbative coupling. The main features of the two cases are summarized in Table I. The evolution chain differed slightly between the two considered cases. Specifically, the chain for Case B extended that of Case A by incorporating more isotopes and reactions. They are illustrated in Figure 4. For both cases, the input microscopic cross sections were derived through spatial homogenization and energy condensation, starting from the JEFF 3.1 library [20], and were obtained using the ECCO cell code [21] available with ERANOS.

TABLE I
Summary of the test cases' characteristics.

	Case A - infinite medium	Case B - finite medium
Geometry	Homogeneous slab	Homogeneous cylinder
Volume V (m^3)	1.00000	9.93900×10^{-1}
Power density ϱ ($MWth/m^3$)	1.25000×10^2	1.25767×10^2
Boundary conditions	Reflection	Void
Evolving isotopes	4	6
Non-evolving isotopes	0	2
Burnable zones	1	1
Non-burnable zones	0	0
Energy groups	1	33
Time steps	24	120
Time step duration (d)	15	15

III.A. Case A - infinite medium

III.A.1. Problem statement

Case A consists of an infinite, homogeneous multiplying medium that incorporates three heavy nuclides (^{238}U, ^{239}Pu and ^{240}Pu), and a unique fission product (^{129}I). The evolution chain involves all four isotopes and undergoes only two radiative captures (n, γ) - from ^{238}U to ^{239}Pu, and from ^{239}Pu to ^{240}Pu - and three fissions producing ^{129}I with a yield $Y = 200\%$. To make the

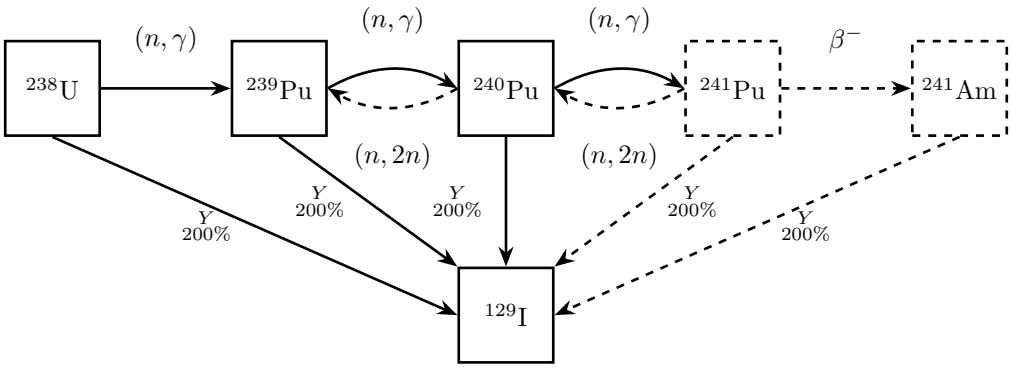

Fig. 4. Evolution chain used to test the ERANOS procedure. Isotopes are boxed, while reactions and decays are represented by arrows. Fissions are indicated through their yield Y. Dashed isotopes, reactions, and decays are present in the finite-medium case only.

problem analytically manageable, several simplifications were implemented. Specifically, a single energy group was considered for discretization, and all microscopic cross sections except for those related to fission and capture were manually set to zero, to exclude them from flux calculations. Case A was modeled using both ERANOS and MATLAB© [22]. In MATLAB©, the problem was represented symbolically using the Symbolic Math Toolbox [23] to seek the analytical solution, importing the ECCO nuclear data into the code. Exploiting a symbolic solver made it possible to perform multiple time steps, leading only to a slight increase in computational time. Therefore, a depletion period of 1 year was divided into 24 time steps of 15 days each. The consistent number of time steps allows for a two-tier comparison between numerical and analytical solutions. Results from the early stages of the direct and adjoint loops should be used to verify the correctness of the ERANOS procedure, while those from the later loop steps (also) indicate how the use of approximated methods producing and being fed with approximated values affects the deviation of the numerical solution from the reference one. In Case A, the power density was set to 125 MWth/m^3, which is in accordance with the value set for ALFRED-like lead-cooled fast reactors [24]. To simulate an infinite medium in ERANOS, reflective boundary conditions were applied to a finite slab of length $l = 1$ m, corresponding to a volume $V = 1$ m^3. This setup, combined with a power P of 125 MWth, achieved the desired thermal power density. Other input data are summarized in Table II. In particular, the initial composition was chosen to have an almost critical reactor, leading to low concentrations of plutonium compared to the standards of fast reactors, with the enrichment $N_{\mathrm{Pu}}/(N_{\mathrm{U}} + N_{\mathrm{Pu}})$ just above 5%. Case A thus describes a strongly breeding

TABLE II
Case A input quantities and their values for different isotopes.

Input Quantity	U238	Pu239	Pu240	I129
N (cm^{-3})	1.06000×10^{22}	4.00000×10^{20}	2.00000×10^{20}	1.00000×10^{4}
$\sigma^{(c)}$ (b)	1.66247×10^{-1}	2.19263×10^{-1}	2.74985×10^{-1}	1.48802×10^{-1}
$\sigma^{(f)}$ (b)	2.86239×10^{-2}	1.57500	3.48740×10^{-1}	0
$\nu\sigma^{(f)}$ (b)	8.04927×10^{-2}	4.64276	1.05740	0
$\sigma^{(\kappa)}$ ($\mathrm{W{\cdot}cm}^2$)	1.03392×10^{-36}	5.01463×10^{-35}	1.13281×10^{-35}	1.71507×10^{-37}
$Q^{(f)}$ (MeV)	1.94764×10^{2}	1.99073×10^{2}	1.99470×10^{2}	0
$Q^{(c)}$ (MeV)	4.80600	6.53300	5.24200	6.50000

reactor.

III.A.2. Results and discussion for direct calculations

The first part of the test focused on calculating direct quantities like the multiplication factor and the flux at each time boundary, as well as the time evolution of concentrations within each depletion step. Since the reactor is homogeneous and infinite, the multiplication factor k_∞ was calculated analytically at each relevant boundary instant t_j using the formula:

$$k_\infty(t_j) = \frac{\left(\vec{\nu} \odot \vec{\sigma}^{(f)}\right) \cdot \vec{N}(t_j)}{\left(\vec{\sigma}^{(c)} + \vec{\sigma}^{(f)}\right) \cdot \vec{N}(t_j)}, \tag{45}$$

where $\odot$ indicates an element-wise multiplication and the vector notation accounts for all isotopes in the reactor. There is no spatial dependence in $\vec{N}$ due to the presence of a single burnable zone. The flux shape remains constant with depletion or position and was simply imposed to be

$$\psi(t_j) = \frac{1}{V} \tag{46}$$

to satisfy the shape flux normalization condition. In the case at hand, due to the infinite homogeneous geometry, the flux shape coincided with its average $\tilde{\psi}(t_j)$, with the latter being the one used in ERANOS to evolve the isotopic concentrations in $[t_j, t_{j+1}]$. The flux intensity was calculated using

$$\phi(t_j) = \frac{\varrho}{\left(\vec{\sigma}^{(\kappa)} \cdot \vec{N}(t_j)\right)\psi(t_j)}, \tag{47}$$

where the power density ϱ at the numerator replaces the actual power P, thus eliminating the need to integrate over (or, in this case, multiply by) the reactor volume V in the denominator. The

scalar neutron flux was then obtained as $\Phi(t_j) = \phi(t_j)\psi(t_j)$. A first indication that the numerical and the analytical approaches are in good agreement is provided by examining some direct output quantities and their relative deviations at t_1 (beginning of the first depletion step), $t_J = t_{f-1}$ (beginning of the last depletion step), and $t_{J+1} = t_f$ (end of depletion), as shown in Table III, with discrepancies being in the region of 10^{-4} to 10^{-6}. Relative deviations ε_q throughout this

TABLE III
Relevant direct output quantities for the infinite medium case, with $f = J + 1 = 25$.

Output Quantity	ERANOS	MATLAB©	Relative deviation
$k_\infty(t_1)$	1.00472	1.00472	0
$k_\infty(t_{f-1})$	1.09244	1.09248	3.66139×10^{-5}
$\Phi(t_1)$ ($\mathrm{cm^{-2}s^{-1}}$)	3.75559×10^{15}	3.75560×10^{15}	2.66269×10^{-6}
$\Phi(t_{f-1})$ ($\mathrm{cm^{-2}s^{-1}}$)	3.28604×10^{15}	3.28620×10^{15}	4.86885×10^{-5}
$N_{^{129}\mathrm{I}}(t_f)$ ($\mathrm{cm^{-3}}$)	2.35702×10^{20}	2.35700×10^{20}	8.48536×10^{-6}
$N_{^{238}\mathrm{U}}(t_f)$ ($\mathrm{cm^{-3}}$)	1.03777×10^{22}	1.03760×10^{22}	1.63982×10^{-4}
$N_{^{239}\mathrm{Pu}}(t_f)$ ($\mathrm{cm^{-3}}$)	5.01334×10^{20}	5.01320×10^{20}	2.79263×10^{-5}
$N_{^{240}\mathrm{Pu}}(t_f)$ ($\mathrm{cm^{-3}}$)	2.03157×10^{20}	2.03150×10^{20}	3.44573×10^{-5}

work are defined by

$$\varepsilon_q = \frac{|q_n - q_a|}{|q_a|}, \tag{48}$$

where q and q_a represent the numerically and analytically calculated values of a generic quantity q. For instance, the null relative deviation for $k_\infty(t_1)$ indicates that, with equal input data, the correct set of microscopic cross sections was set to 0 in ERANOS. On the other hand, the very small relative deviations at t_J suggest that, at least for the direct loop, the ERANOS intermediate results propagate throughout the depletion period with negligible impact. This indirectly highlights that the forward loop is constructed correctly in ERANOS.

III.A.3. Overview of the adjoint calculations

In MATLAB©, the adjoint Bateman equation was easily derived from the matrix form of the direct Bateman equation by transposing the transmutation and decay matrices and inverting the sign of the time derivative. Three response functionals were studied: the final concentrations of the three heavy nuclides involved. The adjoint problem was modeled by imposing a partial perturbative coupling which involved both the Bateman and the Power normalization equations. The numerical and analytical results were then compared in terms of adjoint concentrations, adjoint power, and Bateman and power indirect sensitivity terms. The Boltzmann constraint was not considered, as

it is irrelevant for Case A: this test was specifically crafted to have null generalized adjoint fluxes $\Gamma^*(t_j)$ and sources $Q^*(t_j)\ \forall j$. This outcome arises from Eqs. (16) and (17), since $\psi(t_j) \neq 0$ from Eq. (46). Interestingly, in the configuration of Case A, Q_j^* is defined by the difference of two terms, i.e. $Q_{j,\mathrm{I}}^*$ and $Q_{j,\mathrm{II}}^*$, which cancel out regardless of the orthonormality condition:

$$Q_j^* = \underbrace{\int_{t_{j+}}^{t_{j+1}^-} \left(\vec{N}^*, \frac{\partial \boldsymbol{T}_j}{\partial \psi_j}\vec{N}\right) dt}_{Q_{j,\mathrm{I}}^*} \underbrace{-P_j^* \phi_j \vec{N}_j \cdot \vec{\sigma}^{(\kappa)}}_{Q_{j,\mathrm{II}}^*}$$

$$= \frac{1}{\psi_j}\int_{t_{j+}}^{t_{j+1}^-} \left(\vec{N}^*, \boldsymbol{T}_j\vec{N}\right) dt - P_j^*\frac{P}{V\psi_j} = \frac{1}{V\psi_j}\int_{t_{j+}}^{t_{j+1}^-} \left\langle \vec{N}^*, \boldsymbol{T}_j\vec{N}\right\rangle_V dt - P_j^*\frac{P}{V\psi_j}$$

$$= \frac{P}{V\psi_j}\left(\frac{1}{P}\int_{t_{j+}}^{t_{j+1}^-} \left\langle \vec{N}^*, \boldsymbol{T}_j\vec{N}\right\rangle_V dt\right) - P_j^*\frac{P}{V\psi_j} = \frac{P}{V\psi_j}P_j^* - P_j^*\frac{P}{V\psi_j} = 0, \tag{49}$$

in which the linearity of the transmutation matrix with respect to the flux magnitude has been exploited. On the one hand, a null Γ_j^* facilitated the analytical approach, which would have otherwise required solving an inhomogeneous integro-differential equation. On the other hand, the computation of Q_j^*, while irrelevant, could be done analytically with ease and, therefore, it was considered valuable for testing the relative ERANOS subroutine. More precisely, the computation aimed at verifying the correct implementation of $Q_{j,\mathrm{I}}^*$ and $Q_{j,\mathrm{II}}^*$ separately, with the former being based on $S_{N,j}$ (as P_j^*, see Eq. (39)), while the latter involving directly P_j^* (see Eq. (34)). Then, the two source terms were also compared with one another.

III.A.4. Results and discussion for adjoint power

The backward evolution of the adjoint power is displayed in Figure 5 for the three response functionals. The maximum values of the relative deviations, on the order of 10^{-3}, indicate good agreement between ERANOS and MATLAB© for all the subcases at all time steps. As expected, the deviations slightly increase as the adjoint calculation progresses, following a linear trend. Examining the adjoint powers, they are almost constant, with a tendency to exhibit higher absolute values at the beginning of depletion. The sign of P_j^* depends on the response functional. This variation is due to the integrand appearing in Eq. (12), in which the adjoint concentrations act as weighting functions. For instance, when the response functional is $R = N_{^{238}\mathrm{U}}(t_f)$, the final

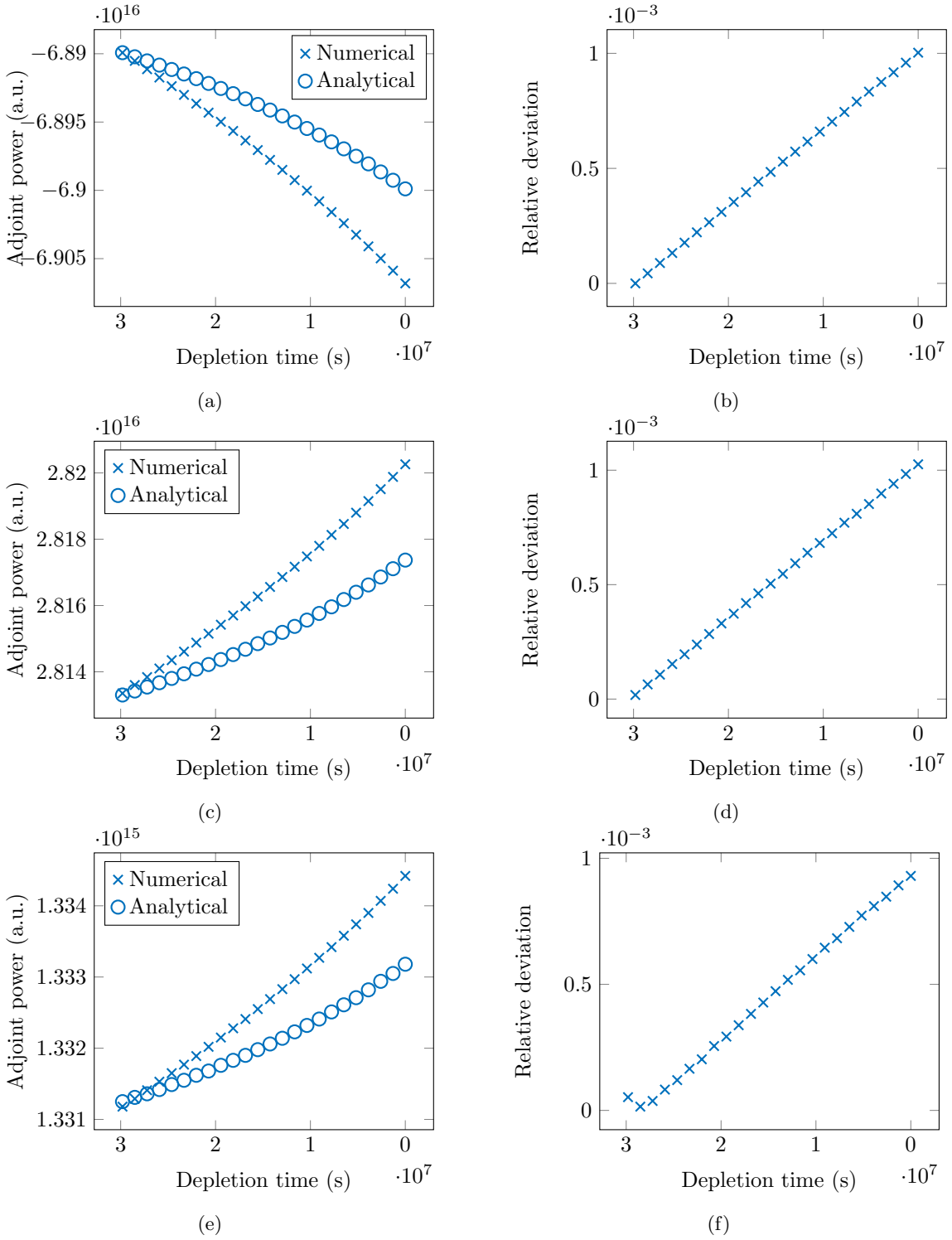

Fig. 5. Time comparison of the actual value and the relative deviation of the numerical Adjoint power with respect to its analytical counterpart. Different response functionals are considered: $N_{^{238}\mathrm{U}}(t_f)$ for (a) and (b), $N_{^{239}\mathrm{Pu}}(t_f)$ for (c) and (d), and $N_{^{240}\mathrm{Pu}}(t_f)$ for (e) and (f), with $f = J + 1 = 25$. Results are shown for $j = f - 1, ..., 1$.

condition on the adjoint concentration of ^{238}U is 1, while it is 0 for the other isotopes:

$$\left.\frac{\partial R}{\partial \vec{N}}\right|_{t_f} = \left[\frac{\partial N_{^{238}\mathrm{U}}(t_f)}{\partial N_{^{238}\mathrm{U}}}, \frac{\partial N_{^{238}\mathrm{U}}(t_f)}{\partial N_{^{239}\mathrm{Pu}}}, \frac{\partial N_{^{238}\mathrm{U}}(t_f)}{\partial N_{^{240}\mathrm{Pu}}}, \frac{\partial N_{^{238}\mathrm{U}}(t_f)}{\partial N_{^{129}\mathrm{I}}}\right]\Bigg|_{t_f} = (1,0,0,0). \tag{50}$$

During the backward loop, the values of the adjoint concentrations change, but only slightly relative to one another. Consequently, the P_j^* integrand is predominantly influenced by the terms that are multiplied by $N^*_{^{238}\mathrm{U}}$. These terms can be derived from the evolution chain in Figure 4. Specifically, they are associated to the ^{238}U Bateman equation and are negative: $-\sigma^{(c)}_{^{238}}\Phi(t_j)N_{^{238}\mathrm{U}}(t) - \sigma^{(f)}_{^{238}}\Phi(t_j)N_{^{238}\mathrm{U}}(t)$. This explains why the adjoint power for $R = N_{^{238}\mathrm{U}}(t_f)$ is negative (as shown in Figure 5(a)) and more intense at the beginning of depletion, where $N_{^{238}\mathrm{U}}$ is higher. A similar approach can be used to analyze the sign of P_j^* for other responses, being aware that the order of magnitude of both direct concentrations and cross sections also plays a role.

III.A.5. Results and discussion for adjoint concentrations

A selection of ERANOS adjoint concentrations at time boundaries ($N^*(t_j^-) = N_j^{*-}$, and $N^*(t_j^+) = N_j^{*+}$, along with the associated jump power term $-P_j^*\Pi_j$) for different responses is displayed in Figure 6 for the perturbative coupled configuration. Figure 6 also includes the corresponding ERANOS sets of uncoupled adjoint concentrations (obtained considering only the Bateman constraint) to highlight the impact of the jump condition. The selection aims to illustrate different behaviors of the adjoint concentrations. Figure 6(a) presents $N^*_{^{238}\mathrm{U}}$ for the case where $R = N_{^{238}\mathrm{U}}(t_f)$, which is the scenario previously analyzed in relation to the sign of P_j^*. The jump term has an order of magnitude of 10^{-4}, leading to adjoint concentrations similar in value (significantly higher than the jump term), which remains close to the final condition value of 1. According to the theory, the sign of the jump term is opposite to that of the associated P_j^*. During the beginning of the depletion period, the adjoint concentration of ^{238}U decreases, as the importance to the final ^{238}U concentration becomes more distributed among other isotopes in the reactor, though ^{238}U remains dominant. Relative deviations between numerical results are below 10^{-3} and increase towards the final backward steps, as anticipated. Notably, some relative deviations for N^{*-} and N^{*+} match between ERANOS and MATLAB© (up to the sixth significant digit), as indicated by the missing marks in Figure 6(b). The time evolution of the adjoint concentration of ^{238}U for $R = N_{^{239}\mathrm{Pu}}(t_f)$, is shown in Figure 6(c). In this case N^* and R refer to different

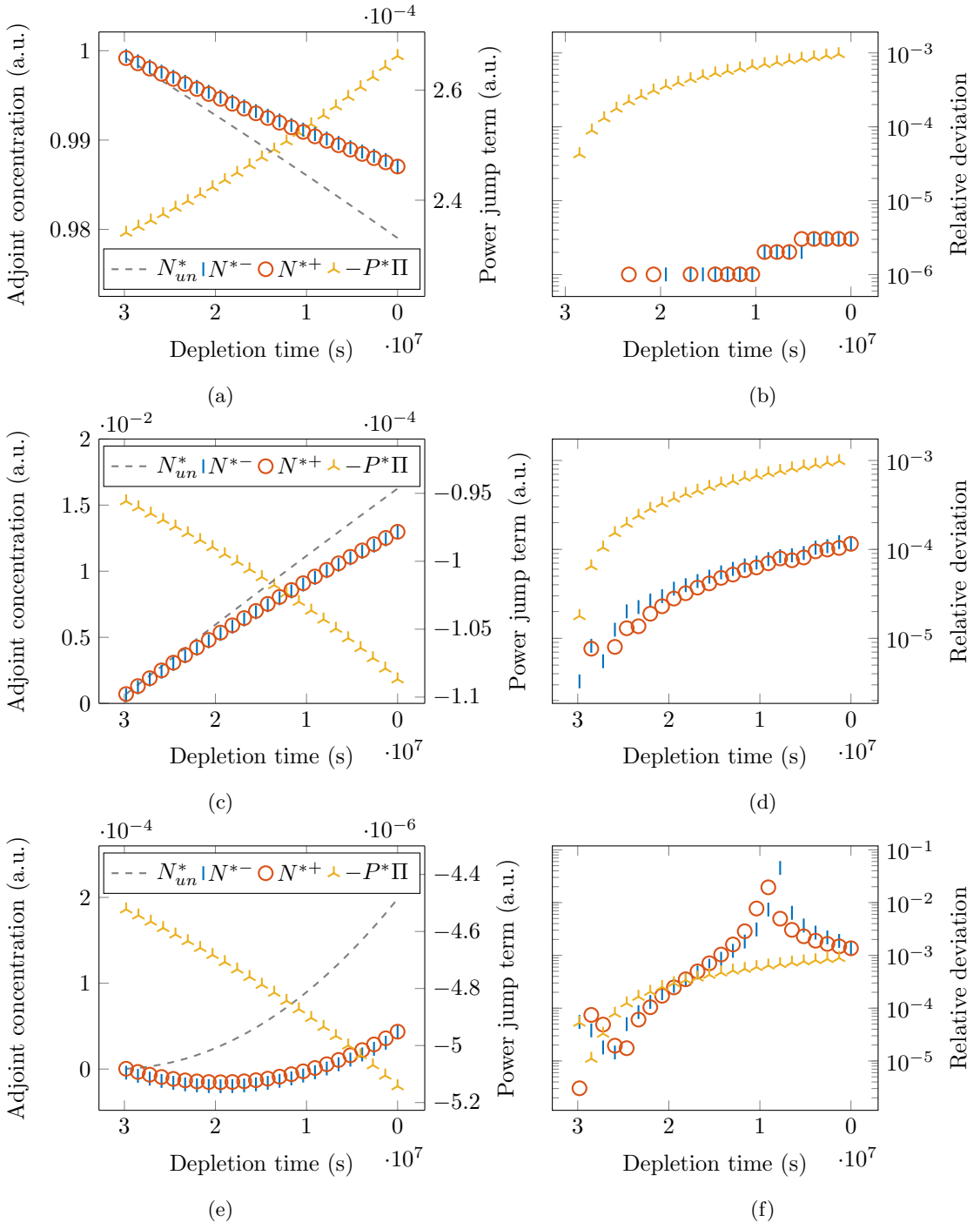

Fig. 6. Time evolution of the actual value of the boundary numerical adjoint concentrations of ^{238}U and the power jump term (see Eq. 21), and time comparison with their relative analytical counterpart (subscript a) in terms of relative deviation. The uncoupled adjoint concentrations (subscript un) are displayed for reference. Different responses are considered: $N_{^{238}\mathrm{U}}(t_f)$ for (a) and (b), $N_{^{239}\mathrm{Pu}}(t_f)$ for (c) and (d), and $N_{^{240}\mathrm{Pu}}(t_f)$ for (e) and (f), with $f = J + 1 = 25$. Results are shown for $j = f - 1, ..., 1$.

isotopes, resulting in $N^*_{^{238}\mathrm{U}}(t_f) = 0$. Despite its relatively small role, the importance of ^{238}U is slightly higher at the beginning of the depletion period. Relative deviations remain below 10^{-3}, with the largest deviations occurring for the jump term. For the first two cases, where adjoint concentrations do not change sign, ε is very small. In contrast, Figure 6(e) illustrates a different situation for $N^*_{^{238}\mathrm{U}}$ for $R = N_{^{240}\mathrm{Pu}}(t_f)$. Since ^{238}U and ^{240}Pu are loosely linked in the evolution chain, the importance of the former on the final concentration of the latter is limited. In the uncoupled case, this results in low values for the evolution of $N^*_{^{238}\mathrm{U}}$, which is only weakly positive (below 2×10^{-4}). In the partially coupled case, the jump power term is of comparable size with the adjoint concentration, but it has the opposite sign. This results in a competitive dynamic that makes $N^*_{^{238}\mathrm{U}}$ experience a sign inversion at around 10^7 s from the beginning of depletion, which is challenging for both ERANOS and MATLAB© to detect simultaneously, especially with the small values involved. This discrepancy corresponds to increased relative deviations ε (between 10^{-1} and 10^{-2}), as shown in Figure 6(f). Away from the inversion region, deviations align more closely with those observed in other cases (below 10^{-3}). This suggests that the discrepancies are not directly linked to the coding in ERANOS, but rather stem from the approximations inherent in its methods for solving the adjoint Bateman equation. Increasing the time discretization in the critical temporal region could mitigate this effect, but it is important to note that the very low values of N^* imply negligible absolute deviations (around 10^{-8}) and, consequently, limited impacts on sensitivities. Therefore, the adjoint concentrations computed by ERANOS are considered acceptable, demonstrating a robust agreement with MATLAB© results despite the noted specific issues.

III.A.6. Results and discussion for the generalized adjoint source

The time evolutions of the two terms forming the generalized adjoint source are plotted in Figure 7, along with their relative deviations, for the same three response functionals. Their behavior follows that of the corresponding adjoint powers, as predicted by Eq. (49), which shows that both the theoretical $Q^*_{j,\mathrm{I}}$ and $Q^*_{j,\mathrm{II}}$ differ from P^*_j only for a multiplicative factor of $P/V\psi_j$. However, since they were calculated using their general formulations, numerical issues sometimes resulted in $Q^*_j \neq 0$ in ERANOS, with values around 10^5 times smaller than those of the single terms, indicating discrepancies at the sixth significant digit and below. Nevertheless, the comparison

between numerical and analytical calculations for each term is favorable, with relative deviations that increase linearly reaching peaks of the order of 10^{-3}. The impact of not respecting the orthogonality condition $\langle Q_j^*, \psi_j \rangle = 0$ should be investigated in the future to analyze, in particular, how this affects Γ^* in problems with full perturbative coupling.

III.A.7. Results and discussion for indirect terms of sensitivity coefficients

When the partial perturbative coupling is involved, there are two indirect terms of the sensitivity coefficient: the Bateman term S_N (also present in the uncoupled configuration) and the power term S_P, which is associated with the power normalization equation. The numerically calculated $|S_N|$ and $|S_P|$ are represented in Figure 8 for different combinations of R and α, along with their analytical values. The choice of considering absolute values was made to adopt a logarithmic scale, which better highlights the different orders of magnitude involved. The corresponding relative deviations (calculated using the actual sensitivities, not their absolute values) are displayed similarly in Figure 9. The most notable relative deviation is that of $S_N(N_{^{240}\mathrm{Pu}}, \sigma^{(f)}_{^{238}\mathrm{U}})$, just above 10^0, but its reference analytical value is the lowest among the computed ones, below 10^{-5}. Further inspection reveals that $\mathrm{sgn}(S_N) \neq \mathrm{sgn}(S_{N,a})$, which seems to be related to the problem encountered in Figure 6(e). Aside from this issue, which is negligible for the reference value's order of magnitude, the other Bateman sensitivity terms reach maximum deviations between 10^{-2} and 10^{-1} for $R = N_{^{238}\mathrm{U}}(t_f)$ and $R = N_{^{240}\mathrm{Pu}}(t_f)$. Instead, the deviations for the power sensitivity term are almost all aligned below 10^{-3}, as the computation of this term is less affected by the time integral used for S_N, which is approximated in ERANOS. In general, these values are deemed acceptable because sensitivity coefficients account for the contributions coming from all the time steps. The errors can also be reduced by increasing the number of time steps or by bettering the time integration of the product between the direct and adjoint concentrations in Eq. (25).

III.B. Case B - finite medium

III.B.1. Problem statement and results of the direct calculations

After verifying the ERANOS procedure through an analytical solution, the problem studied in Case A was expanded and made more complex, leading to the formulation of Case B, which was only modeled using ERANOS. This time, the reactor is a homogeneous finite cylinder characterized

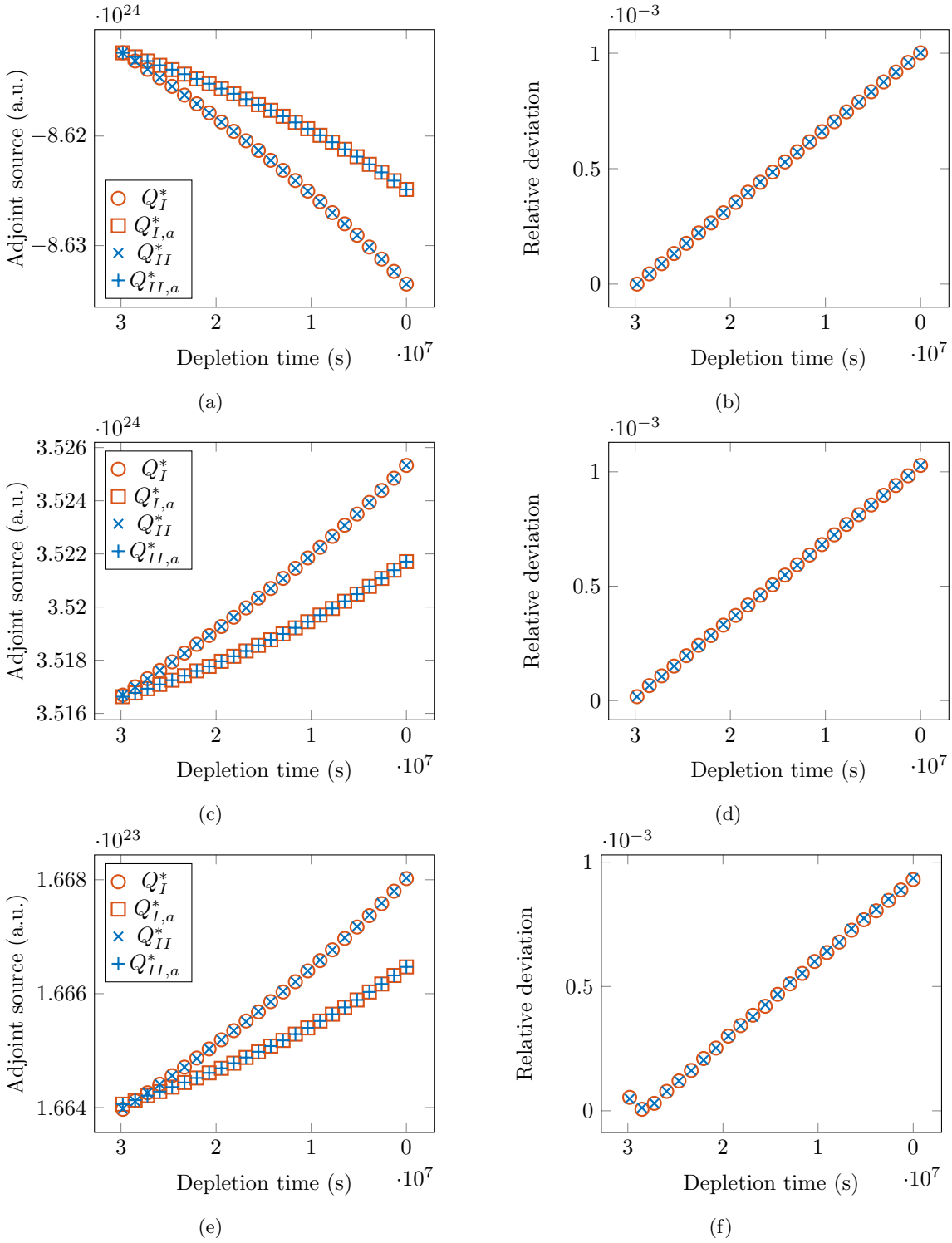

Fig. 7. Time comparison of the actual value and the relative deviation of the numerical generalized adjoint source terms with respect to their analytical counterparts (subscript a). Different response functionals are considered: $N_{^{238}\mathrm{U}}(t_f)$ for (a) and (b), $N_{^{239}\mathrm{Pu}}(t_f)$ for (c) and (d), and $N_{^{240}\mathrm{Pu}}(t_f)$ for (e) and (f), with $f = J + 1 = 25$. Results are shown for $j = J, ..., 1$.

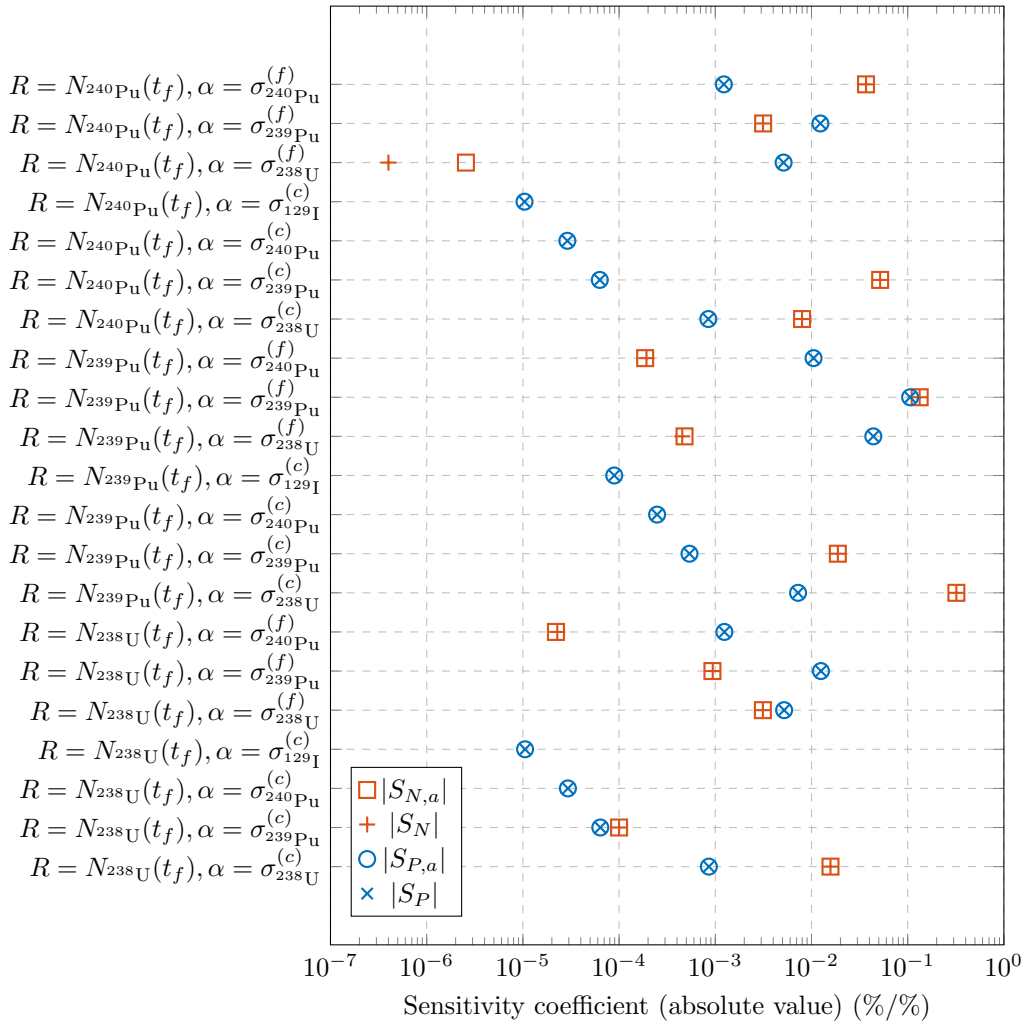

Fig. 8. Comparison between the numerical 1-group Bateman and power sensitivity terms (in absolute value) and their analytical counterparts (subscript a) for different combinations of responses R and input parameters α.

by a radius $r = 0.78$ m and a height $h = 0.52$ m, so to have a volume of approximately 1 m^3 and a power density slightly above 125.0 MWth/m^3 (achieved by setting $P = 125.0$ MWth), therefore very close to that of case A. To better capture the neutron physics, a 33-group energy discretization suited for fast reactor applications [25] was adopted, and the previous hypothesis of including only fissions and capture reactions in flux calculations was removed. The evolution chain was expanded to include also additional isotopes and reactions (dashed in Figure 4). In particular, the extension includes ^{241}Pu and ^{241}Am, $(n, 2n)$ reactions, additional captures and fissions, and a β^- decay. Moreover, two non-evolving isotopes were considered, namely ^{56}Fe and

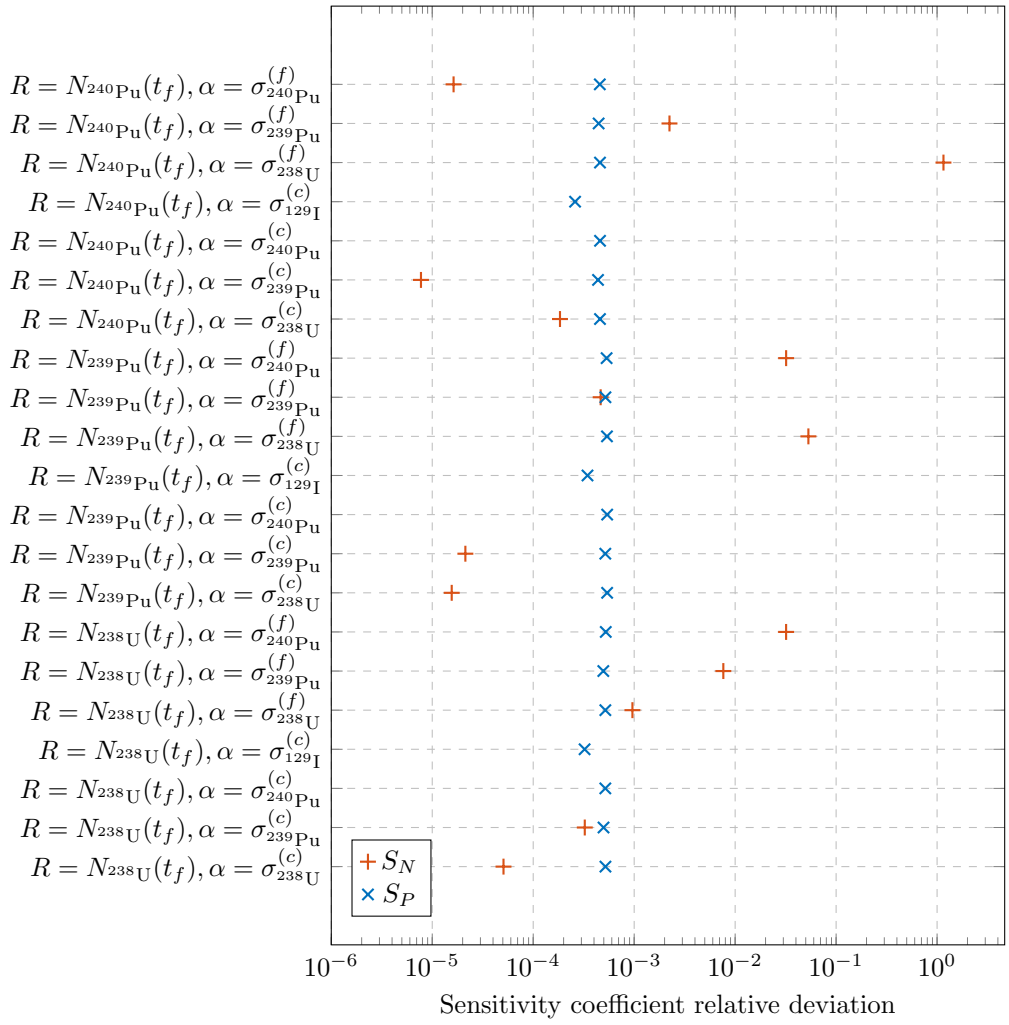

Fig. 9. Relative deviation of the numerical 1-group Bateman and power sensitivity terms from their analytical counterparts for different combinations of responses R and input parameters α.

^{208}Pb, whose nature required a specialized treatment during the writing of the ERANOS procedure. The single burnable zone configuration was retained from Case A. However, since the procedure was equipped to handle also multiple burnable and non-burnable zones, this feature is planned for future testing. The depletion period was extended to 5 years and divided into 120 steps of 15 days each, therefore keeping the same step length of Case A. The initial isotopic concentrations, as well as the ones calculated at the end of depletion, are collected in Table IVwhere it can be seen the much higher enrichment used in Case B, compared to Case A, so to make the system close to critical at beginning of life (close to 35 at.%); this has resulted in a burner reactor. For

reference, the multi-group fluxes averaged over the whole reactor at t_1 and t_{f-1} are plotted in Figure 10, where it can be seen that the flux intensifies over time, but with the peak remaining in the energy bin between 4.98×10^5 eV and 8.21×10^5 eV (group 7). The corresponding values of the multiplication factor are $k_1 = 1.00459$ and $k_{f-1} = 7.51844 \times 10^{-1}$ where the strong decrease dictated by the enrichment selected can be observed. The objective of Case B was to show the

TABLE IV
Initial and final direct concentrations for the finite medium case, with $f = J + 1 = 121$.

Isotope	$N(t_1)$ (cm^{-3})	$N(t_f)$ (cm^{-3})
^{56}Fe	8.60290×10^{20}	8.60290×10^{20}
^{129}I	4.00000×10^{3}	1.22495×10^{21}
^{208}Pb	7.60000×10^{21}	7.60000×10^{21}
^{238}U	2.43556×10^{21}	2.24673×10^{21}
^{239}Pu	8.20400×10^{20}	5.05893×10^{20}
^{240}Pu	3.87608×10^{20}	3.03963×10^{20}
^{241}Pu	8.74320×10^{19}	5.14715×10^{19}
^{241}Am	1.89432×10^{19}	2.94089×10^{19}

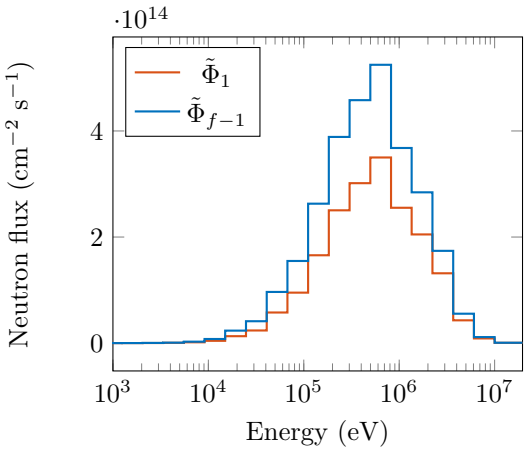

Fig. 10. Zone-averaged 33-group scalar neutron flux as a function of energy at the beginning of the first ($j = 1$) and the last ($j = f - 1$) depletion steps, with $f = J + 1 = 121$. For visualization purposes, the flux is displayed only for energies above 10^3 eV.

effects and the relevance of considering a partial perturbative coupling of the burnup equations, in particular about the the sensitivity coefficients. With 33 energy groups, a full coupling would have involved $Q_j^* \neq 0$ and $\Gamma_j^* \neq 0$. However, since the newly implemented routine for the calculation of the generalized adjoint source has yet to be verified, only the Bateman and the power normalization equations were used as constraints on R. Similarly to Case A, the response functions were chosen to be the final isotopic concentrations of the evolving heavy nuclides. The sensitivity coefficients

were computed with respect to fission, (n,γ), and $(n,2n)$ microscopic cross sections of all eight involved nuclides. Additionally, the calculations were repeated for the perturbatively uncoupled case to draw comparisons.

III.B.2. Preliminary considerations on the sensitivity coefficients

Some representative sensitivity coefficients are shown in Figure 11 as a function of energy. Four indirect sensitivity terms are included: the uncoupled Bateman term $S_{N,un}$, the coupled Bateman term S_N, the coupled power term S_P, and the coupled total term $S_{tot} = S_N + S_P$. In general, the different intensities of the sensitivities in the various energy bins are (also) influenced by a combination of the zone-averaged neutron flux (see Figure 10) and the multi-group microscopic cross sections assigned to α. Note that the total sensitivity coefficient in the uncoupled case is identical to $S_{N,un}$ because there is no direct term for any combination of the selected responses and input data. Before analyzing the single plots, a few preliminary considerations are necessary. Firstly, the computed adjoint powers were negative for all responses, with values ranging approximately from -10^{14} to -10^{16}. Consequently, all S_P terms should be non-negative, as they represent the sum, over all t_j, of the instantaneous power production rates of a given isotope through α, weighted with $-P^* > 0$. Regarding S_N, each time step contribution accounts for the time-integrated evolution of all transmutation reaction rates involving α, weighted with $\vec{N}^*(t)$ (this indirectly involves the jump condition). Therefore, the sign of S_N is more complex to predict and should be investigated on a case-by-case basis.

III.B.3. Results and discussion for sensitivity coefficients

Figure 11(a) shows the sensitivity of $N_{^{239}\mathrm{Pu}}(t_f)$ to the multi-group capture cross section of ^{238}U. From the perspective of the evolution chain, a positive input perturbation on $\sigma^{(c)}_{^{238}\mathrm{U}}$ results in a higher production rate of ^{239}Pu, as reflected by the Bateman term both with and without coupling. The peaks occur for E between 4.98×10^5 eV and 8.21×10^5 eV (corresponding to energy group 7, as for the fluxes in Figure 10) and are close to 3×10^{-2}. The positive propagation of the perturbation is also evident by looking at the generic $S_{N,j,g}$ term, which in this case is:

$$S_{N,j,g} = \frac{1}{N_{^{239}\mathrm{Pu}}(t_f)} \int_{t_{j+}}^{t^-_{j+1}} \left(N^*_{^{239}\mathrm{Pu}}(t) - N^*_{^{238}\mathrm{U}}(t)\right)\tilde{\Phi}_g(t_j)\sigma^{(c)}_{^{238}\mathrm{U},g} N_{^{238}\mathrm{U}}(t)\, dt. \tag{51}$$

The integrand involves the reaction rate that transmutes ^{238}U into ^{239}Pu, and $N^*_{^{239}\mathrm{Pu}}(t) - N^*_{^{238}\mathrm{U}}(t) > 0$, as the importance of ^{239}Pu is close to 1. In the coupled case the power jump term is positive (it features $-P^*_j$) and therefore increases both adjoint concentrations. However, overall $\sigma^{(\kappa)}$ prevails for ^{239}Pu over ^{238}U, so $N^*_{^{239}\mathrm{Pu}}(t) - N^*_{^{238}\mathrm{U}}(t)$ is increased by the coupling, ultimately leading to $S_N > S_{N,un}$. Similar arguments apply because $N^*_{^{238}\mathrm{U}}$ is much smaller than $N^*_{^{239}\mathrm{Pu}}$, making the net effect of the perturbative coupling an increase in $N^*_{^{239}\mathrm{Pu}}$. Since capture is less influential than fission for power production, S_P is almost negligible compared to S_N, as evidenced by the generic $S_{P,j,g}$ term

$$S_{P,j,g} = -\frac{P^*_j}{N_{^{239}\mathrm{Pu}}(t_f)} \tilde{\Phi}_g(t_j) \sigma^{(c)}_{^{238}\mathrm{U},g} \frac{\partial \sigma^{(\kappa)}_{^{238}\mathrm{U},g}}{\partial \sigma^{(c)}_{^{238}\mathrm{U},g}} N_{^{238}}(t_j), \tag{52}$$

in which the fission contributions in $\sigma^{(\kappa)}_{^{238}\mathrm{U},g}$, although small for fissionable isotopes like ^{238}U compared to fissile material, have been removed by the partial derivative. Consequently, the total sensitivity in the coupled case is higher than in the uncoupled one due to the power jump term, but remains very close to S_N because S_P is approximately 2 orders of magnitude smaller than S_N for nearly all groups. In Figure 11(b), the response and the input data pertain to the same isotope, with R remaining unchanged and $\alpha = \sigma^{(f)}_{^{239}\mathrm{Pu}}$. Consequently, the orders of magnitude involved are higher compared to Figure 11(a), with some terms reaching absolute values above 10^{-1}. The primary mechanism by which ^{239}Pu can reduce its concentration is through fission, which is reflected in the strong negative values of the Bateman term, both with and without coupling. Examining the j-th Bateman term

$$S_{N,j,g} = \frac{1}{N_{^{239}\mathrm{Pu}}(t_f)} \int_{t_{j+}}^{t^-_{j+1}} \left(Y N^*_{^{129}\mathrm{I}}(t) - N^*_{^{239}\mathrm{Pu}}(t) \right) \tilde{\Phi}_g(t_j) \sigma^{(f)}_{^{239}\mathrm{Pu},g} N_{^{239}\mathrm{Pu}}(t)\, dt, \tag{53}$$

and noting that ^{129}I has minimal impact on the final concentration of ^{239}Pu, the focus can be put on $N^*_{^{239}\mathrm{Pu}}$. The power jump term is positive, resulting in $N^*_{^{239}\mathrm{Pu}} > N^*_{^{239}\mathrm{Pu},un}$. Consequently, the absolute value of the weighting function in Eq. (53) is higher in the coupled case. This, combined with the negative sign in front of $N^*_{^{239}\mathrm{Pu}}$, leads to $S_N < S_{N,un}$.The power sensitivity term is positive, as anticipated with $P^*_j < 0$, and its magnitude is comparable to that of the Bateman term. This reflects the high fission cross section of ^{239}Pu, and highlights a significant difference from S_P of Figure 11(a). The competitive effects of $S_N < 0$ and $S_P > 0$ result in an overall lower total sensitivity in the coupled case than in the uncoupled one. This indicates that the depletion

of ^{239}Pu is less sensitive to input perturbations in its fission cross section than what is predicted by the uncoupled perturbation theory. In the remaining two panels of Figure 11 there are two similar scenarios, where the sensitivity coefficients are predominantly influenced by the power term. Both scenarios involve the ^{239}Pu and ^{241}Am isotopes, which are weakly coupled in the adopted evolution chain. Specifically, ^{241}Am can be reached through two (n,γ) reactions, linking ^{239}Pu, ^{240}Pu and ^{241}Pu, followed by a β^- decay of the latter. However, this path is unidirectional, meaning that in Case B is not possible to trace back from ^{241}Am to ^{239}Pu. This limitation affects the sensitivity coefficients. Figure 11(c) was obtained with $R = N_{^{239}\mathrm{Pu}}(t_f)$ and $\alpha = \sigma^{(f)}_{^{241}\mathrm{Am}}$. The formula for the generic Bateman term is:

$$S_{N,j,g} = \frac{1}{N_{^{239}\mathrm{Pu}}(t_f)} \int_{t_{j^+}}^{t^-_{j+1}} \left(Y N^*_{^{129}\mathrm{I}}(t) - N^*_{^{241}\mathrm{Am}}(t)\right) \tilde{\Phi}_g(t_j) \sigma^{(f)}_{^{241}\mathrm{Am},g} N_{^{241}\mathrm{Am}}(t)\, dt. \tag{54}$$

In the decoupled case, ^{239}I and ^{241}Am are irrelevant, as their reactions do not lead to the formation of ^{239}Pu, resulting in $S_{N,j,g,un} = 0\ \forall j, g$. This absence of $S_{N,un}$ is reflected in Figure 11(c). In contrast, the coupled case introduces the power jump term making the adjoint concentrations non-zero, and leading to small negative values of S_N, with magnitude around 10^{-4}. The negative sign arises because ^{241}Am contributes more to the power than ^{129}I, so the jump term for $N^*_{^{241}\mathrm{Am}}(t)$ is larger, influencing the sign of the weighting function in Eq. (54). The total sensitivity is positive but slightly smaller than S_P due to the influence of S_N. Its magnitude peaks just above 10^{-3}, and is significantly lower than those compared to the sensitivities shown in Figure 11(a) and Figure 11(b). When the scenario is reversed, having $R = N_{^{241}\mathrm{Am}}(t_f)$ and $\alpha = \sigma^{(f)}_{^{239}\mathrm{Pu}}$, the resulting sensitivities are showed Figure 11(d). This time, S_N is nonzero in both cases, although it is negligible due to the very low quantities of ^{239}Pu that indirectly transmute into ^{241}Am. Interestingly, in the decoupled case S_N is positive, as expected since $N^*_{^{241}\mathrm{Am}}$ can originate from ^{239}Pu. However, when coupling is enabled, the negative power jump term affects the results, leading to S_N being negative. This last example demonstrates that the choice of the evolution chain influences not only the direct evolution of the core but also the behavior of the sensitivity coefficient terms.

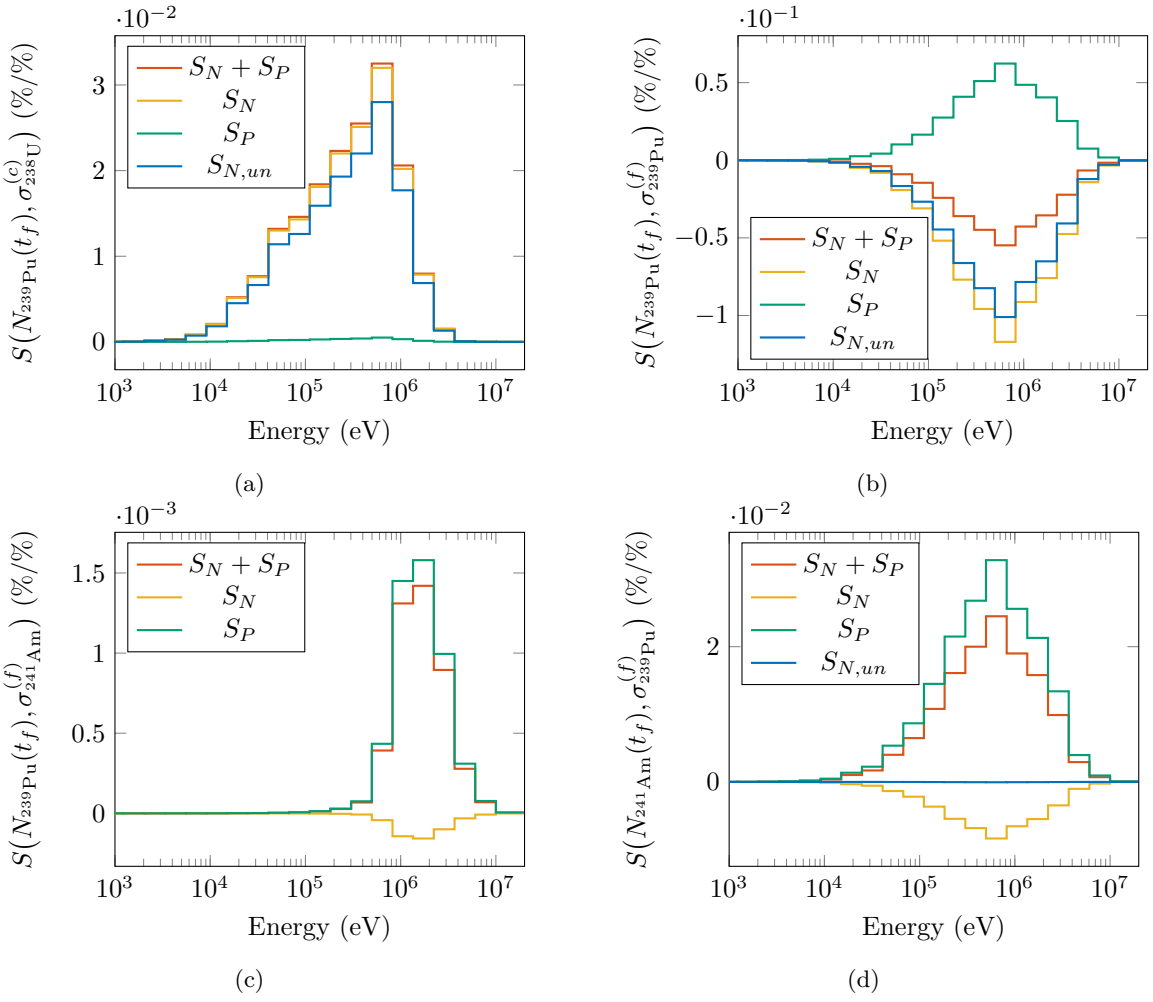

Fig. 11. End-of-depletion 33-group sensitivity coefficient terms for different sets of response functionals and input parameters, in both partially coupled and fully decoupled cases: $N_{^{239}\mathrm{Pu}}(t_f)$ and $\sigma^{(c)}_{^{238}\mathrm{U}}$ for (a), $N_{^{239}\mathrm{Pu}}(t_f)$ and $\sigma^{(f)}_{^{239}\mathrm{Pu}}$ for (b), $N_{^{239}\mathrm{Pu}}(t_f)$ and $\sigma^{(f)}_{^{241}\mathrm{Am}}$ for (c), $N_{^{241}\mathrm{Am}}(t_f)$ and $\sigma^{(f)}_{^{239}\mathrm{Pu}}$ for (d).

IV. CONCLUSIONS AND PERSPECTIVES

A novel procedure was implemented in the deterministic suite ERANOS 2.3N, on the basis of a variational approach of GPT, to overcome its current limitations in calculating sensitivity coefficients in depletion problems, which are of great importance for the design of nuclear reactors. In particular, a partial perturbative coupling was achieved by implementing the power normalization constraint in addition to the existing Bateman constraint. The new procedure, which focuses on final isotopic concentrations as response functionals, introduces several innovative elements. These

include subroutines for the adjoint power, the first-order power sensitivity term, and the calculation of the power jump term for updating the adjoint concentration vector. The implementation of the adjoint power leverages formal similarities with the Bateman sensitivity term, for which ERANOS already had dedicated functions. Similarly, the generalized adjoint source was also implemented, despite being part of the full perturbative coupling, whose complete integration into ERANOS is still ongoing. The new procedure was initially verified for a simple case for which an analytical solution was computed through a MATLAB© script utilizing the Symbolic Math Toolbox. The results for direct and adjoint quantities showed generally very good agreement, with most relative deviations consistently below 10^{-3}. A few larger discrepancies were found, but they proved to be not significant (being related to negligible quantities) and attributable to ERANOS inherent approximated methods. A second, more complex test case was then studied, using exclusively ERANOS, to compare the decoupled and the partially coupled configurations primarily through the multi-group indirect sensitivity coefficient terms. Various sensitivities were considered to highlight different physical phenomena. In general, the adjoint power proved to be a significant contribution to the overall sensitivity coefficients, both through the power sensitivity term and the power jump term, which ultimately impacted the Bateman sensitivity term. Moving forward, the goal is to extend the outlined ERANOS procedure to achieve full perturbative coupling of the burnup equations, to improve the computation of time integrals involving direct and adjoint concentrations to better account for short-lived nuclides, and to implement other useful response functionals for reactor design. Among these, it is worth citing the End-Of-Cycle effective multiplication factor k and the reactor reactivity swing. These improvements are aimed at optimizing reactor operation and fuel management, potentially enhancing the economic performance and safety of nuclear reactors.

DISCLOSURE STATEMENT

The authors report there are no competing interests to declare.

REFERENCES

[1] M. L. Williams, "Development of depletion perturbation theory for coupled neutron/nuclide fields," *Nuclear Science and Engineering*, **70**, *1*, 20 (1979).

[2] T. Takeda and T. Umano, "Burnup sensitivity analysis in a fast breeder reactor—part I: sensitivity calculation method with generalized perturbation theory," *Nuclear Science and Engineering*, **91**, *1*, 1 (1985).

[3] W. S. Yang and T. J. Downar, "Generalized Perturbation Theory for Constant Power Core Depletion," *Nuclear Science and Engineering*, **99**, *4*, 353 (1988).

[4] W. Yang and T. Downar, "Depletion perturbation theory for the constrained equilibrium cycle," *Nuclear science and engineering*, **102**, *4*, 365 (1989).

[5] A. Gandini, "Generalized perturbation theory (GPT) methods. A heuristic approach," *Advances in Nuclear Science and Technology: Festschrift in Honor of Eugene P. Wigner*, **19**, 205 (1987).

[6] A. Gandini, "The heuristically-based generalized perturbation theory," *EPJ-Nuclear Sciences & Technologies*, **7** (2021).

[7] B. Murphy and C. Perfetti, "Depletion perturbation theory sensitivity coefficients in Monte Carlo simulations," *Proceedings of the international conference on physics of reactors-PHYSOR 2022* (2022).

[8] J. Leppänen, M. Pusa, T. Viitanen, V. Valtavirta, and T. Kaltiaisenaho, "The Serpent Monte Carlo code: Status, development and applications in 2013," *Annals of Nuclear Energy*, **82**, 142 (2015).

[9] D. Portinari, Y. Calzavara, L. Chabert, and A. Bidaud, "Depletion perturbation theory: a sensitivity tool for the high flux reactor conversion to low enriched uranium," *Proceedings of the international conference on physics of reactors-PHYSOR 2022* (2022).

[10] D. Portinari, Y. Calzavara, L. Chabert, and A. Bidaud, "A 3 Regions model for LWR fuel pin sensitivity analysis with depletion perturbation theory," *Proceedings of the international conference on physics of reactors-PHYSOR 2022* (2022).

[11] D. Schneider, F. Dolci, F. Gabriel, J.-M. Palau, M. Guillo, and B. Pothet, "APOLLO3® CEA/DEN deterministic multi-purpose code for reactor physics analysis," *PHYSOR 2016–Unifying Theory and Experiments in the 21st Century* (2016).

[12] S. Lahaye, P. Bellier, H. Mao, A. Tsilanizara, and Y. Kawamoto, "First verification and validation steps of MENDEL release 1.0 cycle code system," *Proc. Int. Conf. PHYSOR2014, Kyoto, Japan* (2014).

[13] N. Linden, A. Tsilanizara, and J. Tommasi, "Depletion Perturbation Theory in decay heat calculation context," *Annals of Nuclear Energy*, **185**, 109743 (2023).

[14] G. Rimpault, D. Plisson, J. Tommasi, R. Jacqmin, J.-M. Rieunier, D. Verrier, and D. Biron, "The ERANOS code and data system for fast reactor neutronic analyses," *PHYSOR 2002-International Conference on the New Frontiers of Nuclear Technology: Reactor Physics, Safety and High-Performance Computing* (2002).

[15] V. G. Peluso, "Sviluppo, validazione e benchmarking del codice di neutronica deterministica ERANOS in rapporto alle metodologie perturbative per l'analisi di sensibilità dei reattori di IV generazione," PhD Thesis, Università di Roma 'La Sapienza' (2015).

[16] W. Khamakhem, "Etude de l'évolution du combustible dans des réacteurs rapides de quatrième génération : impact des données nucléaires sur leur performance," PhD Thesis, Université Paris-Sude XI U.F.R Scientifique d'Orsay (2010).

[17] L. Buiron and D. Plisson-Rieunier, "Nuclear data propagation with burnup: impact on SFR reactivity coefficients," *Proc. Int. Conf. ICAPP17* (2017).

[18] J. Tommasi, "ERANOS User's Manual, Application of Perturbation Theory with Finite Difference Diffusion and Sn Transport Flux Solvers," SPRC/LEPh 07-003, CEA.

[19] G. Rimpault, D. Honde, and J. M. Rieunier, "ERANOS: Manuel des Methodes. Transferts Internes de Données Nucléaires," NT-SPRC-LEPh-93-252, CEA (1999).

[20] A. Koning, R. Forrest, M. Kellett, R. Mills, H. Henriksson, Y. Rugama, O. Bersillon, O. Bouland, A. Courcelle, M. Duijvestijn et al., "The jeff-3.1 nuclear data library-jeff report 21," , Organisation for Economic Co-operation and Development (2006).

[21] G. Rimpault, "Physics documentation of ERANOS, the ECCO cell code," RT-SPRC-LEPh-97-001, CEA (1997).

[22] T. M. Inc., *MATLAB© version: 9.13.0.2193358 (R2022b) Update 5*, Natick, Massachusetts, United States (2022).

[23] T. M. Inc., *Symbolic Math Toolbox version: 9.2 (R2022b)*, Natick, Massachusetts, United States (2022).

[24] G. Grasso, C. Petrovich, D. Mattioli, C. Artioli, P. Sciora, D. Gugiu, G. Bandini, E. Bubelis, and K. Mikityuk, "The core design of ALFRED, a demonstrator for the European lead-cooled reactors," *Nuclear Engineering and Design*, **278**, 287 (2014).

[25] G. Palmiotti, M. Salvatores, M. Assawaroongruengchot, M. Herman, P. Oblozinsky, and C. Mattoon, "Nuclear data target accuracies for generation-IV systems based on the use of new covariance data," , Idaho National Lab. (INL), Idaho Falls, ID (United States) (2010).